4.3.5 Interplanetary dust

Eberhard Grün, Valeri Dikarev

4.3.5.1 Introduction

Dust is finely dispersed solid material in interplanetary space. It derives from a number of sources: larger meteoroids, comets, asteroids, the planets, their satellites, and rings, and there is interstellar dust sweeping through the Solar System. These dust particles are also often called micrometeoroids, and range in size from assemblages of a few molecules to tenth millimeter-sized grains, above which size they are called meteoroids.

Dust particles strongly interact with their environment. Impacts of dust particles onto other solid objects cause cratering or even fragmentation and generation of secondary ejecta particles. Interplanetary dust particles are charged by the photo effect from solar UV flux and by interaction with the solar wind. Because of their small sizes forces additional to solar and planetary gravity affect their trajectories. Radiation pressure and the interactions with ubiquitous magnetic fields disperse dust particles in space away from their sources.

Dust particles absorb and scatter solar radiation and emit thermal radiation giving rise to Zodiacal light at visible wavelengths and thermal emission at infrared wavelengths. Astronomical observations of both emissions provide information on the average properties of a very large number of particles and their spatial distribution. Figure 1 shows a comparison of various methods to characterize dust in interplanetary space.

Information on the physical and chemical characteristics and the orbital motion is obtained by direct methods. Direct methods include [01Aue]:

- In-situ measurements of individual particles by instruments on board satellites and space probes,
- Investigations of dust impact craters on natural surfaces like on lunar samples and man-made impact plates returned from space, and
- Collection of dust particles on collectors on spacecraft returned to Earth and on airplanes in the stratosphere.

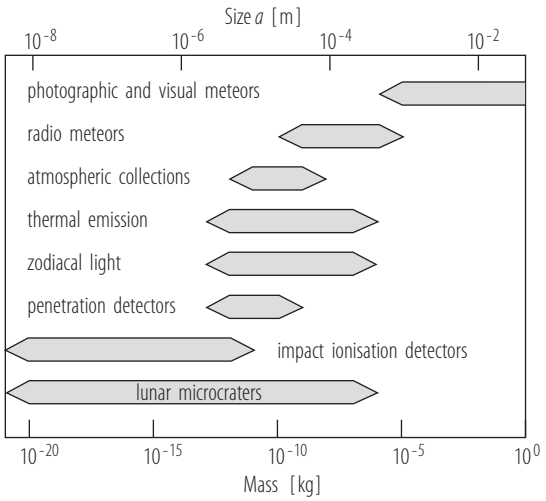

Fig. 1. Comparison of meteoroid sizes and masses covered by different observational methods.

Meteor observations refer generally to big meteoroids and hence are not covered here. There are several review books that describe the development of the field over the last years [85Gie, 91Lev, 96Gus, 01Gru1, 02Gre, 06Kru1].

4.3.5.2 Measurement techniques

4.3.5.2.1 In-situ measurements

Three types of impact detectors were mainly used for interplanetary dust measurements: momentum sensors, penetration detectors and impact ionisation detectors [01Aue]. Momentum sensors measure the momentum transferred from the dust particle to an impact plate by a piezo-electric sensor. Because of their susceptibility to environmental effects (temperature variations and energetic particle radiation) they are only successfully applied with low sensitivities ($> 10^{-8}$ g) in high dust flux environments like close to comets (Table 1). Penetration detectors record the mechanical destruction from a dust particle's impact, e.g. the penetration of a 25 or 50 μm thick steel film which corresponds to a detection threshold of 10^{-9}or 10^{-8}g (approx. 10 μm radius) at a typical impact speed of 20 km/s. At lower impact speeds the minimum detectable particle mass is bigger and vice versa. A more sensitive penetration detector is the PVDF (PolyVinylidine Fluoride) film [85Sim]. PVDF is a polarized material. When a dust particle impacts the film, it excavates some polarized material and generates an electric signal which is then detected. The pulse height of the signal is a function of the mass and speed of the dust particle. A typical measurement range is from 10^{-11} to 10^{-8} g (1 to 10 μm radius).

The most sensitive dust detectors are impact ionisation detectors. Figure 2 shows a schematic diagram of the dust detector flown on the Cassini spacecraft [04Sra]. The detector has an aperture of 0.1 m^2 and is based on the impact ionisation effect: A dust particle that hits the hemispherical target in the back at speeds above 1 km/s will produce a partially ionised vapor cloud. The ions and electrons of the cloud are separated in an electric field within the detector and collected by various electrodes. The amplitude and the wave form of the signal are measures of the mass and speed of the impacting particle (Fig. 3) [89Gru, 95Gru1]. The central part of the Cassini detector is a time-of-flight (TOF) mass spectrometer: a high electric field between the target and a grid 3 mm in front of the target accelerates the ions to high energy (1000 eV). During the flight between the grid and the ion collector ions of different masses separate and arrive at different times at the multiplier. In this way a mass spectrum is measured which represents the elementary composition of the dust grain. Entrance grids in front of the target measure any electric charge of dust particles. Dust analyzers incorporating a mass spectrometer have been flown on the Helios spacecraft, the Giotto and VEGA missions to comet Halley, the Stardust mission to comet Wild 2, and on the Cassini mission to Saturn (Table 2). While linear TOF mass spectrometers reach mass resolutions $M/\Delta M \leq 50$ mass analyzers (Fig. 4) employing a reflectron reach mass resolutions $M/\Delta M \geq 100$ which is sufficient for isotopic analyses. Electrostatic dust accelerators are used to calibrate these detectors with micron and submicron-sized projectiles at impact speeds of up to about 100 km/s [01Aue]. Based on the experience from previous dust instruments a novel dust telescope has been developed and is ready for new applications in space. The dust telescope consists of a trajectory sensor and a large-area-mass-analyzer, LAMA, of 0.1 m^2 sensitive area. The trajectory sensor determines via induced electric charges precision dust trajectories before the grains impact LAMA. LAMA is a reflectron mass analyzer with a mass resolution $M/\Delta M > 100$ [05Sra, 06Sra1, 06Sra2, 07Ste, 05Gru].

Table 1. Characteristics of in-situ dust measurements flown in interplanetary space. Distance ranges are those in which dust measurements were obtained. Detector types are momentum sensors (MS), penetration detectors (PD), and impact ionisation detectors (II) and analyzers (IA). The mass thresholds refer to 20 km/s impact speed. The effective solid angles correspond to the sensor field-of-view, and the dynamic measurement range refers to the mass determination.

Mission, instrument	Distance range [AU]	Detector type	Mass threshold [g]	Sensitive area [m^2]	Solid angle [sr]	Dynamic range	Refs.
Helios 1	0.3-1	IA	9×10^{-15}	0.012	1.23	10^4	[73Die]
Galileo	0.7-5.4	II	4×10^{-15}	0.1	1.4	10^6	[92Gru1, 95Gru2]
Pioneer 9	0.75-0.99	II	2×10^{-13}	0.0074	2.9	200	[69Ber]
VeGa 1, 2	0.79-0.83				n.a.		[85Sag]
DUCMA		PD	10^{-11}	0.0075		10^3	[85Per]
PUMA		IA	2×10^{-15}	0.0005		10^6	[86Kis1]
SP-1		II	2×10^{-15}	0.0081		10^5	[87Gru]
SP-2		MS,II	10^{-11}	0.05		10^8	[85Sag]
Giotto	0.86				n.a.		
DIDSY		MS	2×10^{-8}	~ 0.1		10^5	[87Gru, 86McD]
PIA		IA	2×10^{-15}	0.0005		10^6	[86Kis1]
Pioneer 8	0.97-1.09	II	2×10^{-13}	0.0094	2.9	200	[69Ber]
HEOS 2	1	II	2×10^{-15}	0.01	1.03	10^4	[73Die]
Hiten	1	II	2×10^{-15}	0.01	1.5	3×10^4	[91Ige]
Nozomi	1-1.4	II	10^{-15}	0.014	1.5	2×10^4	[98Ige]
Stardust							
CIDA		IA	2×10^{-15}	0.0086	0.3	10^6	[03Kis]
DFMI		MS,PS	10^{-5},10^{-12}	0.7,0.02	6	10^8	[03Tuz]
Ulysses	1-5.4	II	4×10^{-15}	0.1	1.4	10^6	[92Gru2]
Pioneer 11	1-10	PD	6×10^{-9}	0.26$^{(1)}$	2.8	1	[80Hum]
Cassini	1-10						
DA		II,IA	2×10^{-15}	0.1	0.6	10^6	[04Sra]
HRD		PD	3×10^{-13}	0.006	3	4×10^4	[04Sra]
Pioneer 10	1-18	PD	8×10^{-10}	0.26$^{(1)}$	2.8	1	[80Hum]
New Horizons	1-40	PD	10^{-12}	0.1	6	10^3	[07Hor]

$^{(1)}$ corresponds to initial value; each impact reduces the sensitive area by $\sim 0.4\%$.

Table 2. Dust analyzers. Mass resolution $M/\Delta M$ gives the highest mass that can be separated from the neighboring mass. References to some significant dust measurements are given.

Mission	Instrument	Type	$M/\Delta M$	Dust measurements
Helios	Dust Analyzers	Linear TOF	5–20	Interplanetary, interstellar dust [81Gru, 06Alt]
Giotto	PIA	Reflectron	> 100	Comet Halley dust [94Fom, 88Jes, 91Jes, 86Kis2, 87Kis, 86Kis3, 87Lan, 92Law, 89Law]
VeGa 1, 2	PUMA	Reflectron	> 100	
Cassini	CDA	Linear TOF	20–50	Interplanetary dust, dust streams, Saturn ring dust [07Hil1, 07Hil2, 05Kem2, 06Pos, 08Pos]
Stardust	CIDA	Reflectron	150	Comet Wild 2, interstellar dust [04Kis, 04Kru]

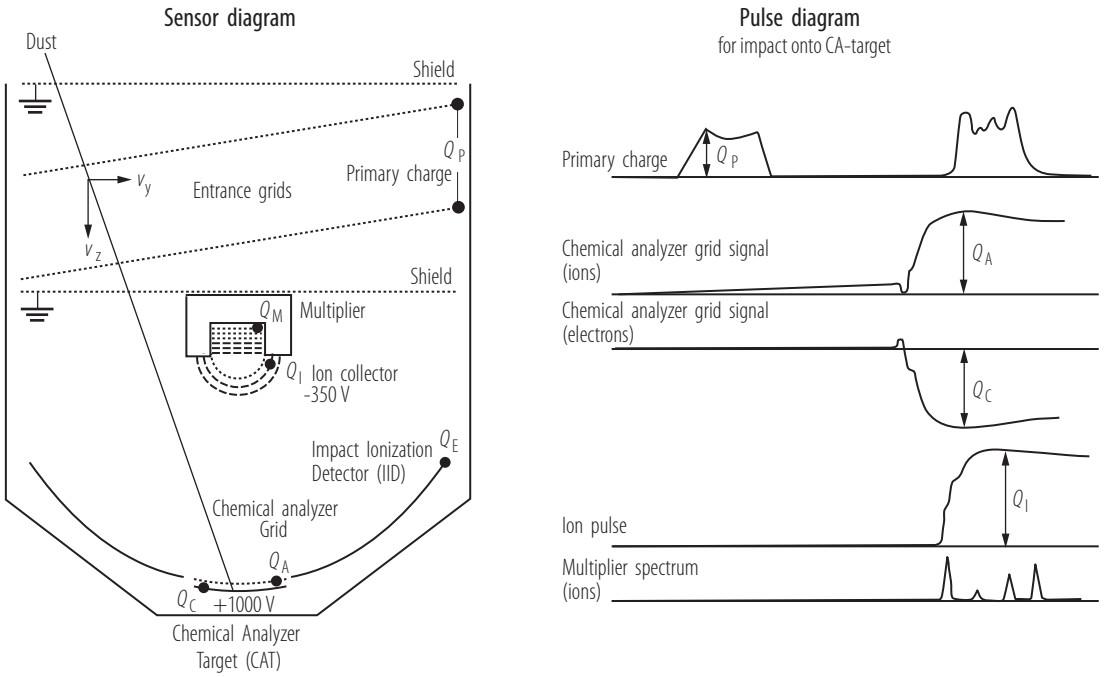

Fig. 2. Schematics of Cassini Dust Analyzer (DA) and schematic signals [04Sra, 01Aue]. Dust particles generate electric pick-up signal while flying through the entrance grids, impact ionisation signals when they hit the target in the back of the detector. A time-of-flight mass spectrum of the released ions is recorded by the multiplier in the ion collector after an impact on the central chemical analyzer target. For further explanations see text.

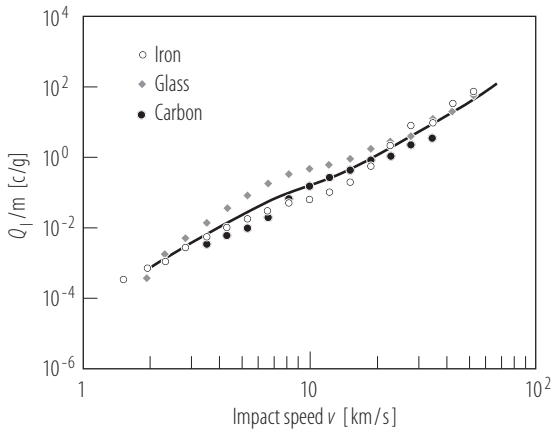

Fig. 3. Calibration of the Galileo and Ulysses dust detectors [89Gru, 95Gru1]. Positive impact charge Q_I normalized to dust particle mass m as function of impact speed v [95Gru2].

4.3.5.2.2 Micro crater studies

Since the return of lunar surface samples by the Apollo and Luna missions the study of impact craters on material exposed to space has been used to characterize the flux of interplanetary micrometeoroids and man made space debris particles. Monitoring the near-Earth dust environment is nowadays a routine activity of all major space agencies. In 1984 NASA released the Long Dura-

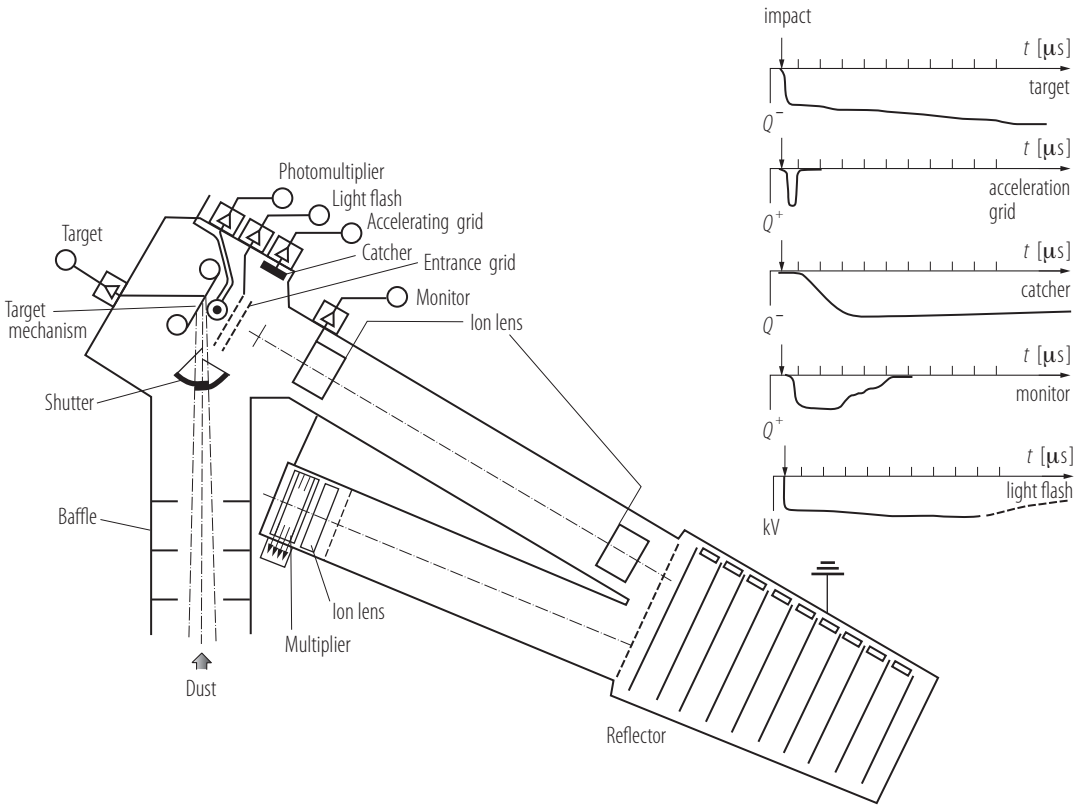

Fig. 4. Dust Mass Analyzer PIA on Giotto: Instrument schematics and signals generated [86Kis1]. Signals recorded from a dust impact onto the target include impact charges and light flash and a mass spectrum of the released ions on the multiplier. A shutter controlled the dust flux onto the target in the high-dust density environment near comet Halley.

tion Exposure Facility, LDEF, into near-Earth space at about 450 km altitude in order to study the effects on materials during the prolonged exposure to space environment. Six years after launch LDEF was retrieved by the Space Shuttle and brought back to the ground. The study of the near-Earth dust environment was also the objective of the European Eureca satellite and of samples from the Russian MIR station which were returned to Earth. Routine inspection of Shuttle windows and the solar arrays returned from the Hubble Space Telescope are used to characterize the damage produced by the meteoroid and debris environment [94Kin, 95Lov1, 98McD, 08Dro].

Craters on fragile materials like lunar rocks or solar cell material display a central cater which is surrounded by a spallation zone from which large chips have been removed. The ratio of the spallation zone diameter to the central pit diameter is quite variable. Laboratory simulations of high velocity impacts have been performed in order to calibrate crater sizes with projectile sizes and impact speeds. The crater diameter to projectile diameter varies from 2 for the smallest microcraters to about 10 for cm-sized projectiles [75Hor, 99Tay]. A difficulty in analyzing the meteoroid flux from crater counts in natural samples like lunar rocks is the generally unknown exposure geometry (e.g. shielding by other rocks) and the exposure time of any surface on a rock. Therefore, the crater size or meteoroid distribution has to be normalized with the help of an impact rate or meteoroid flux measurement obtained by other means (like by in-situ detectors).

4.3.5.2.3 Dust sample return

The NASA Stardust mission [03Bro] was the first space mission designed to return extraterrestrial material from interplanetary space. The primary goal of Stardust was to collect dust samples during its flyby of Comet Wild 2 in January 2004. The spacecraft flew through the coma at a speed of 6.1 km/s within 236 km from the nucleus. Additionally, during its interplanetary cruise the Stardust spacecraft collected samples of interstellar dust. Comet and interstellar particles are collected in aerogel of 50 and 20 kg/m^3 density, respectively [03Tso]. The collector consisted of 0.1 m^2 aerogel and of 0.015 m^2 aluminium foil. Micron-sized dust particles were stopped in the aerogel without much destruction, forming a several millimetre long track. Since aerogel is mostly transparent these tracks are used to find the tiny particles. The aerogel was packed in a Sample Return Capsule which was released from the spacecraft just before re-entry, for a landing on a parachute. On January 15, 2006 the capsule was safely recovered and since then the samples are analysed [06Bro].

4.3.5.2.4 Atmospheric collection

Since 1981, interplanetary dust collection by airplanes has been routinely performed by NASA using high-flying aircraft, which can cruise at 20 km altitude for many hours. On its wings it carries several 100 cm^2 large flat-plate dust collectors which sweep huge amounts of air because of the high speed of the airplane, thereby providing a strong concentration effect. Dust particles stick to the collector surfaces that are coated with silicone oil. After several hours of exposure the collector is retracted into a sealed storage container and returned to the laboratory. After removal of the particles from the collector plate, the silicone oil is washed-off and the particles are preliminarily examined and catalogued. Individual interplanetary dust particles can be ordered for further scientific investigation.

Extraterrestrial grains of about 5 to 50 microns in diameter are collected that way. The lower size-limit is caused by contamination of smaller terrestrial particles. Micron and submicron-sized particles from volcanic eruptions can reach these altitudes in significant amounts. Another type of interference is caused by man-made contamination: about 90% of all collected particles in the 3 to 8 micron size range are aluminum oxide spheres which are products of solid rocket fuel exhausts. The upper limit is caused by the low abundance of bigger particles which are mostly burned up during atmospheric entry at about 100 km altitude. Smaller particles are more gently decelerated in the more tenuous atmosphere at higher altitudes [98Rie, 01Jes].

In the size regime of stratospheric collections (diameters of 5 to 50 μm) a strong selection effect operates in favor of low geocentric velocity particles (and hence by inference of those of asteroidal origin) over those of higher velocities. This "filter" is critical to interpretation of the surviving fraction we collect in or below the atmosphere and to the fraction which can be captured into Earth orbit.

4.3.5.2.5 Meteor radars

Meteoroid dust enters the atmosphere at speeds between 11 and about 70 km/s. Between altitudes of 70 to 120 km this dust generally completely ablates to form an ionised train called a meteor. Meteors can be detected optically ("by eye", telescope, small camera, and TV camera) and by radio waves, the latter being the most sensitive method to detect meteoroids.

Since the early 1940s the properties of meteors have been measured by ground-based radars. Radar detection relies on scattering by the electrons in the meteor train of a radio signal in the approximate frequency range 5 - 500 MHz. For a returned "echo" to be received by most meteor radars, the transmitted beam must strike the meteor train perpendicularly; this is the so-called

"specular" condition and arises from the diffraction properties of the scattered energy. From the atmospheric trajectory of an ablating meteoroid the heliocentric orbit of the body can be determined. Since scattering of radio waves by the ionisation trail in the atmosphere allows us to observe meteors even during the day this method is best suited to perform surveys of the Earth's meteoroid environment. Three major surveys have been performed to date: the US Harvard Radio Meteor Project (HRMP) survey of the 1960s [72Coo, 75Sek, 95Tay, 98Tay], a survey by the New Zealand Advanced Meteor Orbit Radar (AMOR) system [01Bag, 04Gal], and the one by the Canadian Meteor Orbit Radar (CMOR) system [05Jon, 04Bro]. The most sensitive and extensive survey was performed by the multi-station AMOR system in the southern hemisphere. Its limiting radio magnitude is +14 (at 40 km/s), corresponding to a 10^{-7} g mass (40 μm diameter) meteoroid. The three-station CMOR system has limiting radio magnitude +7.

4.3.5.2.6 Remote sensing of the Zodiacal cloud

Only less than 10% of the incident Sun light is scattered by interplanetary dust and contributes to the zodiacal light. The rest of the absorbed energy (>90%) is re-emitted as thermal infrared radiation [01Lev].

The brightness of zodiacal light arrives from the light scattered by a huge number of particles along the line of sight (LOS, see Fig. 5). The scattering angle, that is the Sun-particle-observer angle, varies systematically along the LOS. For one particle the scattered light intensity is a strong function of the scattering angle. For particles larger than the wavelength of the scattered light this scattering function is strongly peaked in the forward direction (scattering angle = 0). Variable particle structure and composition affect the scattering function as well. Therefore, the observed zodiacal brightness is a mean value, averaged over all sizes, compositions and structures of particles along the LOS. Because of the strong influence of the average scattering function (the detailed function is not known) observations from the Earth are generally not sufficient to derive uniquely the spatial density of interplanetary dust. Zodiacal light measurements from interplanetary spacecraft provided radial brightness profiles from which the spatial density distribution can be derived. Pioneer 10 provided observations [76Han] outward from the Earth orbit to 3.3 AU while Helios observations [87Lan] covered radial distances inward to 0.3 AU. The spatial density of particles can be directly derived in case observations are performed along the same LOS from two different positions [85Dum], e.g. for an observer on the Earth when the LOS crosses the Earth's orbit a second time. Then the brightness difference corresponds to the particles along the section of the LOS between the two observations. Zodiacal light is linear polarized, i.e. the brightness intensity I_1 perpendicular to the scattering plane is generally different to the intensity I_2 parallel to the

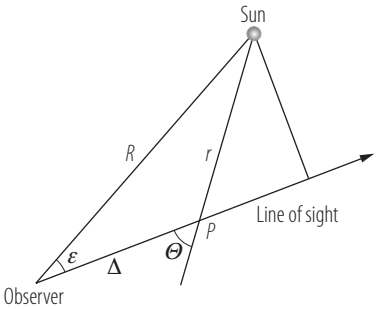

Fig. 5. Observing geometry of zodiacal light measurements. Geometric relations in the scattering plane are defined by the positions of observer, the Sun and the dust particle P. The brightness along the line of sight depends on the elongation angle ϵ or helio-ecliptic longitude $(\lambda - \lambda_\odot)$. The contribution by a single particle depends on the scattering angle θ.

Table 3. Zodiacal light brightness, measured from the Earth near the wavelength of 0.55 μm, in 10^{-8} W m^{-2} sr^{-1} μm^{-1}. The directions are defined by their ecliptic latitude (β) and helio-ecliptic longitude ($\lambda - \lambda_\odot$), once the corrections for the slight inclination of the symmetry plane and for the Earth's orbit eccentricity have been made [80Lev, 98Lei].

β / $\lambda - \lambda_\odot$	0°	5°	10°	15°	20°	25°	30°	45°	60°	75°	90°
0°				3090	1590	970	630	271	147	98	76
5°				2900	1510	930	615	267	147	98	76
10°			4660	2430	1450	850	580	260	146	98	76
15°	11350	6680	3390	1830	1100	745	515	247	144	98	76
20°	6300	4410	2370	1390	895	625	447	233	139	97	76
25°	3780	2780	1700	1080	735	535	403	219	134	96	76
30°	2440	1840	1200	830	605	460	359	204	129	93	76
35°	1630	1250	895	670	505	391	315	190	123	92	76
40°	1170	930	685	525	409	333	277	176	118	91	76
45°	895	720	550	435	350	287	246	164	115	88	76
60°	500	435	346	287	239	205	180	132	102	84	76
75°	333	312	265	223	193	169	149	115	92	81	76
90°	255	241	222	190	164	145	130	102	84	78	76
105°	209	207	194	168	147	131	117	94	81	76	76
120°	185	183	174	151	136	123	111	88	76	73	76
135°	176	175	164	145	132	120	108	88	76	72	76
150°	176	175	163	146	135	125	115	94	78	71	76
165°	193	189	176	163	149	139	129	102	81	71	76
180°	227	209	192	175	160	146	132	103	82	71	76

scattering plane. The degree of polarization is given by $p = \frac{(I_1 - I_2)}{(I_1 + I_2)}$. Historically, the zodiacal light visible brightness V is given in S_{10}(V) units, i.e. brightness equivalent to one 10th magnitude solar-type star per square degree:

$$1S_{10}(\mathrm{V}) = 1.261 \times 10^{-8}\ \mathrm{W\ m^{-2}\ sr^{-1}}\mu\mathrm{m}^{-1} \text{ at } 0.55\mu\mathrm{m}.$$

Above about 1 μm wavelength the intensities in the solar spectrum rapidly decrease. The zodiacal light spectrum follows this decrease until about 5 μm wavelength above which the thermal emission of the dust particles prevails. The maximum of the thermal infrared emission from the zodiacal dust cloud lies between 10 μm and 20 μm. Because of the strong foreground emission and absorption by the Earth atmosphere this infrared emission can only be observed from space. Extensive surveys of the thermal zodiacal emission were provided by the IRAS, ISO and COBE satellites [84Hau, 02Lei, 98Kel2]. Because of the strong solar thermal affects satellite observations have, generally, been performed only in the narrow elongation range 60 to 120°.

4.3.5.3 Observations

4.3.5.3.1 Zodiacal light

Zodiacal light is visible to the naked eye as a faint oval cone of light above the horizon in the evening about one hour after sunset and in the morning before sunrise, around the Sun's position on the celestial sphere (below the horizon). The brightness increases strongly towards the Sun and, as suggested by the name, towards the ecliptic plane. This strong increase towards the Sun is

mostly due to the systematically smaller scattering angle at this observation geometry. However, some brightness increase especially at near infra-red wavelengths is attributed to the enhanced dust density (F corona [04Man]) at small heliocentric distances (< 0.1 AU). In observing zodiacal light from space, at low solar elongations, stray light suppression is essential. Far from the Sun the separation of the star background limits the accuracy. For ground-based observations, additional atmospheric effects (extinction, scattering, and airglow) have to be corrected for.

The spectrum of the zodiacal light follows the solar spectrum closely between 0.2 and 2 μm, including the Fraunhofer lines [98Lei]. Slight deviations reveal the motion of dust particles with respect to the observer. Analyses of the Doppler shifts have been made [84Eas, 96Cla, 08Ipa], but low radial velocities and averaging effects due to the integration over the line of sight make the problem difficult.

The zodiacal light is generally smooth, with some minor features. For an Earth-bound observer, small seasonal oscillations are noticeable. Annual variations of up to 10% are known at high and medium ecliptic latitudes, explained by a small inclination of the symmetry plane of the cloud to the ecliptic plane as well as by Earth's orbit eccentricity [78Dum]. The inclination is rather small ($1.5 \pm 0.4°$), thus the determination of the ascending node is subject to high uncertainty ($96 \pm 15°$). Table 3 lists the zodiacal light brightnesses over the celestial sphere, corrected for the seasonal oscillations.

The zodiacal light is partially linearly polarized, with the electric field vector either parallel or perpendicular to the scattering plane [96Lev]. The polarization degree depends mainly on the solar elongation and reaches the maximum at low angles. It is almost independent on wavelength, except for a slight decrease in the near infrared. This trend has been noticed for light scattered by regoliths.

4.3.5.3.2 Thermal emission

In contrast to its modest appearance in the visual light, the zodiacal dust is a dominant source of diffuse emission at the infrared wavelengths from 5 to 100 μm, except perhaps near the galactic plane [98Lei]. The thermal emission is isotropic, whereas the light scattering is not. It is therefore easier to determine the spatial structure of the dust cloud in the infrared than in the visual wavelengths.

Zodiacal thermal emission at 1 AU is characterized by an approximately blackbody spectrum with temperatures between 255 and 300 K, based on the ISO observations obtained at solar elongations from 60° to 120° [02Lei]. The variation of the temperature can be explained by the geometrical distribution of dust in the inner Solar System and a gradual decrease of the equilibrium temperature of dust with heliocentric distance.

Seasonal variations of the visual brightness have an infrared counterpart. However, the amplitude of the variations is higher, reaching 30% at 12 μm wavelength [98Kel1]. They are also interpreted as a result of the motion of the Earth with respect to the dust cloud's symmetry plane. Based on the COBE infrared survey data, inclination of $2.03 \pm 0.017°$ and ascending node of $77.7 \pm 0.6°$ were determined. Table 4 contains the infrared brightness of zodiacal dust over celestial sphere, corrected for the seasonal oscillations, in the format of Table 3.

The advantage of the infrared observations over the visual ones in resolving the spatial structure of the zodiacal cloud has been proven in several fascinating findings. Trails of meteoroids generated in recent (a few thousands years ago) bursts of cometary activity were discovered as long and narrow features along the orbits of several short-period comets [86Syk, 92Syk, 07Rea]. Their optical depths of $\sim 10^{-8}$ are an order of magnitude smaller than that of the zodiacal cloud. They are composed of rather large, mm-sized particles.

Thermal emission from dust bands at low ecliptic latitudes has also been detected, with the parallaxes (due to the motion of the Earth-bound observatory) pointing to the asteroid belt as

Table 4. Thermal emission by zodiacal dust, measured from an Earth-bound orbit near the wavelength of 12 μm by the COBE infrared telescope at solar elongations > 80°, and extrapolated to shorter elongations using the model [98Kel1], in 10^{-8} W m^{-2} sr^{-1} μm^{-1}. The directions are defined as in Table 3.

β / $\lambda - \lambda_\odot$	0°	5°	10°	15°	20°	25°	30°	45°	60°	75°	90°
0°					156	111	85	49	35	28	24
5°				245	155	110	84	49	35	28	24
10°				244	155	110	84	48	35	28	24
15°	2130	1018	438	238	152	108	83	48	34	28	24
20°	1303	791	391	225	147	106	82	48	34	28	24
25°	870	612	340	208	140	103	80	47	34	28	24
30°	616	477	292	189	132	98	77	46	34	28	24
35°	456	376	250	170	123	93	74	45	33	27	24
40°	349	300	214	153	113	88	71	44	33	27	24
45°	275	244	184	136	104	83	67	43	32	27	24
60°	152	142	120	98	80	67	57	39	31	27	24
75°	97	93	84	72	63	55	48	36	29	26	24
90°	69	67	62	56	50	45	41	32	28	25	24
105°	52	51	49	45	42	38	35	29	26	25	24
120°	43	42	40	38	36	33	31	27	25	24	24
135°	37	36	35	34	32	30	29	25	24	23	24
150°	33	33	32	31	29	28	27	24	23	23	24
165°	31	31	30	29	28	27	26	24	23	23	24
180°	30	30	29	29	27	26	25	23	22	23	24

the location of the source of emission [84Low]. Collisions between asteroids were suggested as the origin of the dust bands [84Der, 90Syk].

4.3.5.3.3 Size distribution at 1 AU

The size distribution of interplanetary dust particles is represented by the lunar microcrater record. Microcraters on lunar rocks have been found ranging from 0.02 μm to millimetres in diameter. Laboratory simulations of high velocity impacts on lunar-like materials have been used to calibrate crater sizes with projectile sizes and impact speeds. The difficulty to derive the impact rate from a crater count on the moon is the generally unknown exposure geometry (e.g. shielding by other rocks) and exposure time of any surface on a rock. Therefore, the crater size or meteoroid distribution has to be normalized with the help of an impact rate or meteoroid flux measurement obtained by other means [85Gru]. In-situ detectors and analyses of impact plates which were exposed on NASA's Long Duration Exposure Facility to the meteoroid flux for several years provided this flux calibration [91Hum, 95Lov2, 98McD].

However, the gravitational well of the Earth enhances the flux of interplanetary dust particles and modifies its velocity distribution. At the top of the atmosphere the mean speed derived from meteor measurements [73Sou, 95Tay] is about 18 km/s and, hence, the meteoroid flux is enhanced [51Opi] by a factor 2 [01McD]. Taking into account this flux increase the total meteoritic mass influx onto the Earth atmosphere is about 40 tons/day [98Kor].

The cumulative interplanetary dust flux at 1 AU and moments of differential spatial density are displayed in Fig. 6 while cumulative moments are given in Table 5. The size distribution of interplanetary dust encountering the Earth peaks at about 200 μm diameter.

Table 5. Moments of the cumulative flux of interplanetary meteoroids at 1 AU: cumulative flux on a spinning flat plate, spatial number density, area density, and mass density.

Grain mass [g]	Cum. flux [m^{-2} s^{-1}]	Cum. number density [m^{-3}]	Cum. area density [m^2/m^3]	Cum. mass density [g/m^3]
1×10^{-18}	2.6×10^{-1}	5.8×10^{-5}	5.3×10^{-19}	9.7×10^{-17}
1×10^{-17}	3.8×10^{-2}	8.4×10^{-6}	5.2×10^{-19}	9.7×10^{-17}
1×10^{-16}	5.9×10^{-3}	1.3×10^{-6}	5.2×10^{-19}	9.7×10^{-17}
1×10^{-15}	1.1×10^{-3}	2.3×10^{-7}	5.2×10^{-19}	9.7×10^{-17}
1×10^{-14}	2.5×10^{-4}	5.4×10^{-8}	5.2×10^{-19}	9.7×10^{-17}
1×10^{-13}	8.3×10^{-5}	1.7×10^{-8}	5.1×10^{-19}	9.7×10^{-17}
1×10^{-12}	3.4×10^{-5}	7.2×10^{-9}	5.1×10^{-19}	9.7×10^{-17}
1×10^{-11}	1.5×10^{-5}	3.1×10^{-9}	5.1×10^{-19}	9.7×10^{-17}
1×10^{-10}	6.4×10^{-6}	1.3×10^{-9}	4.9×10^{-19}	9.7×10^{-17}
1×10^{-9}	3.0×10^{-6}	6.3×10^{-10}	4.7×10^{-19}	9.6×10^{-17}
1×10^{-8}	1.2×10^{-6}	2.5×10^{-10}	4.2×10^{-19}	9.5×10^{-17}
1×10^{-7}	3.0×10^{-7}	6.5×10^{-11}	3.1×10^{-19}	9.0×10^{-17}
1×10^{-6}	4.7×10^{-8}	1.0×10^{-11}	1.7×10^{-19}	7.5×10^{-17}
1×10^{-5}	4.6×10^{-9}	1.0×10^{-12}	6.9×10^{-20}	5.3×10^{-17}
1×10^{-4}	3.3×10^{-10}	7.5×10^{-14}	2.1×10^{-20}	3.2×10^{-17}
1×10^{-3}	1.9×10^{-11}	4.4×10^{-15}	5.5×10^{-21}	1.7×10^{-17}
1×10^{-2}	9.7×10^{-13}	2.3×10^{-16}	1.3×10^{-21}	8.3×10^{-18}
1×10^{-1}	4.7×10^{-14}	1.1×10^{-17}	2.9×10^{-22}	3.9×10^{-18}
1×10^{0}	2.2×10^{-15}	5.2×10^{-19}	6.3×10^{-23}	1.8×10^{-18}
1×10^{1}	1.0×10^{-16}	2.4×10^{-20}	1.4×10^{-23}	8.5×10^{-19}
1×10^{2}	4.7×10^{-18}	1.1×10^{-21}	2.9×10^{-24}	3.9×10^{-19}

In low-Earth orbit micron-sized natural meteoroids are outnumbered (by approximately a factor 3) by man-made space debris. However, there is a strong dependence of the debris flux on the exposure geometry and altitude. Craters produced by space debris particles are identified by chemical analyses of residues in the craters [05Kea]. Residues have been found from space materials and signs of human activities in space like e.g. paint flakes, plastics, aluminum, titanium, and human excretion.

4.3.5.3.4 Chemical and physical properties

4.3.5.3.4.1 In-situ measurements

Helios: interplanetary and interstellar grains. The Helios spacecraft carried two dust analyzers: the ecliptic sensor which was covered by a thin film, and the open south sensor. Although, both sensors had widely overlapping field-of-views the south sensor recorded significantly higher impact rates at otherwise similar impact parameters (impact direction and charge). A comparison with penetration studies showed that particles which did not penetrate the entrance film must have had bulk densities below 1 g/cm^3. Approximately 30% of the particles on high eccentricity orbits ($e > 0.4$) have had such low densities [80Gru, 80Pai].

The Helios dust analyzers were calibrated with a wide range of projectile materials ranging from iron over various minerals to carbonaceous material. The impact spectra obtained between

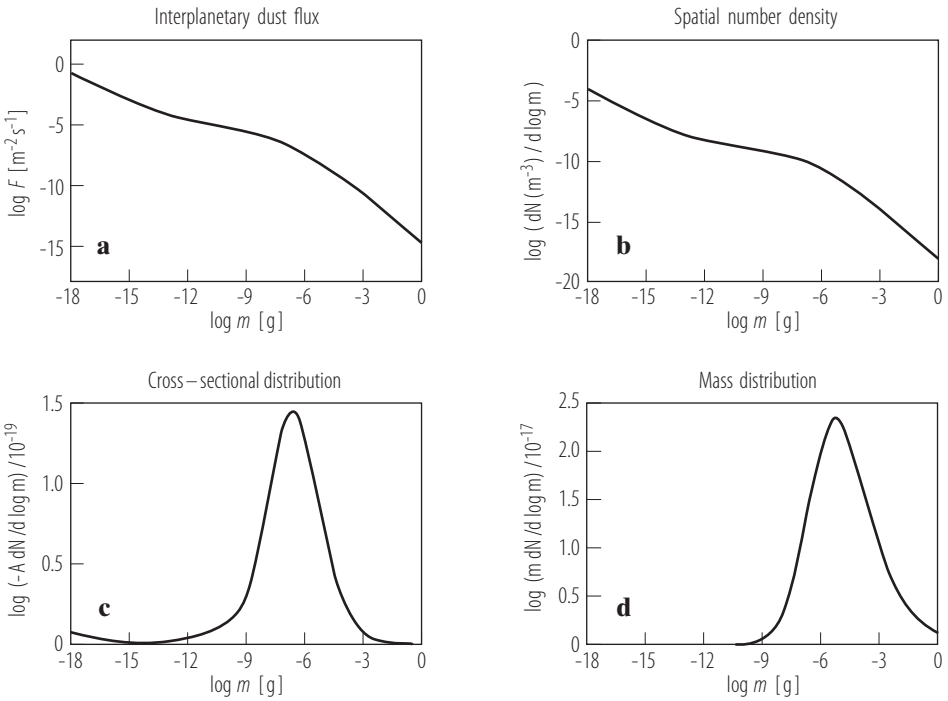

Fig. 6. Moments of the interplanetary dust flux at 1 AU: a) Cumulative flux [m^{-2} s^{-1}] of interplanetary meteoroids on a spinning flat plate at 1 AU distance from the Sun, b) differential spatial density [m^{-3}], differential area density [m^2 m^{-3}], and differential mass density [g m^{-3}].

1 and 0.3 AU from the Sun were classified into three categories: chondritic-type (45%), iron-type (35%), and unidentified (20%). Interstellar particles amounted to 10% of these particles and did not display significantly different compositions [77Dal, 81Gru, 06Alt].

Giotto and VeGa: comet Halley dust. Measurements by all three impact spectrometers onboard the Halley missions Giotto and VeGa 1 and 2 showed that in some spectra ions of the light elements H, C, N, O had the highest intensity peaks, while other spectra were dominated by ions of the rock-forming elements like Mg, Si, Ca, and Fe. The cometary dust particles represented by those spectra were called CHON and SILICATES, respectively. However, the term SILICATES appears to be too narrow since this category contains also Fe-sulfides, metal particles, etc. No grain consists purely of CHON or purely of SILICATES material and because even the smallest cometary particles appear to be fine scale mixtures of carbonaceous and inorganic phases, the proportion of the end member components is varying from grain to grain. This finding led to the interpretation that cometary grains are composed of a silicate core covered by an organic refractory mantle [87Kis]. About half the particles had an abundance ratio of carbon to any rock-forming elements between 0.1 and 10. About one quarter of the particles had smaller ratios and one quarter bigger ratios [01Sek, 94Fom, 88Jes, 91Jes, 86Kis2, 87Kis, 86Kis3, 87Lan, 92Law, 89Law].

SILICATE particles (depleted in organic material) dominate the outer regions of the coma, while CHON and mixed particles are relatively more abundant closer to the nucleus. This observation indicates that the less refractory fraction of the organic component is lost from the grains as they spend some time in the coma [94Fom].

Isotopic information was obtained only for a few among the most abundant elements in the mass spectra of the grains: C, Mg, Si, S, and Fe. The isotopic ratios — within large uncertainties — are generally normal. A clear indication of an isotopic anomaly has been found only for light carbon $^{12}C/^{13}C$ ratios that are much higher than the normal value of 89 and range up to 5000 [87Sol].

In order to gain more insight into the nature of the refractory organic component, statistical

Table 6. Average atomic abundances of elements in Halley's dust and carbonaceous CI chondrites (normalized to Mg abundance) [88Jes].

Element	Halley dust	CI	Halley/CI
H	2,025	492	4.1
C	814	70.5	11.6
N	42	5.6	7.5
O	890	712	1.3
Na	10	5.3	1.9
Mg	=100	=100	1.0
Al	6.8	7.9	0.9
Si	185	93	2.0
S	72	47.9	1.5
K	0.2	0.35	0.5
Ca	6.3	5.68	1.2
Ti	0.4	0.22	1.9
Cr	0.9	1.25	0.7
Mn	0.5	0.88	0.6
Fe	52	83.7	0.6
Co	0.3	0.21	1.2
Ni	4.1	4.59	0.9

Table 7. Mineralogical composition of Halley's SILICATES dust [97Sch].

Mineral group	Estimated proportion	Mineral chemistry	Possible minerals
Mg silicates	>60%	Fe-poor, Ca-poor	Mg-rich pyroxene and/or olivine
Fe sulfides	30%	Some Ni-rich	Pyrrhotite, pentlandite
Fe metal	4-6%	Ni-Poor	Kamacite
Fe oxide	<3%		Magnetite

analyses have been performed of the residuals that remained after the peaks due to the obvious atomic ions had been removed from the spectra. Some of the residual peaks were identified with complex molecular ions and a number of organic-substance classes were therefore inferred to be present in cometary dust [87Kis]. However, an alternative explanation of these peaks in the mass spectra was that they were caused by random impacts of very small, attogram grains [89Sag, 90Utt] and hence, carry no compositional information.

The average bulk mineral component is in agreement with solar elemental abundance (CI-chondrite) except for an excess of organic compounds H, C, N (Table 6) [88Jes, 87Lan]. The mineralogical composition of Halley dust (Table 7) resembles that of stony and iron meteorites [97Sch].

Cassini: interplanetary dust, dust streams. On the path to Saturn Cassini analyzed interplanetary particles, and Jupiter and Saturn dust stream particles (Table 8). Two particles analyzed in interplanetary space at 0.9 and 1.8 AU showed iron to be a major component, being by far the most abundant metal in both particles [07Hil1]. At distances less than 2 AU from Jupiter CDA detected and analyzed Jovian dust stream particles [06Pos]. Their sizes were about 10 nm and their impact speeds were $\sim$ 300 km/s. The spectra showed that alkali salts (NaCl, KCl, K_2SO_4) were dominant particle components, confirming their origin in Io's volcanic plumes. Saturnian dust stream particles are of siliceous composition with occasional water ice mantles indicating their source in the Saturnian rings [05Kem2]. Within the Saturnian system water ice is

Table 8. Spectra characteristics and inferred particle compositions of particles analyzed by the Cassini CDA instrument in interplanetary space. The Rhodium in the spectra originates from the target of the dust analyzer.

Dust species	Spectra characteristics	Inferred particle composition
IDP [07Hil1]	Fe^+, Rh^+ dominant H^+, C^+, O^+ Strong $RhFe^+$ cluster	Iron-rich mineral Little or few silicate and pyrite Pure Iron/Nickel or Iron-rich carbonaceous mineral or oxides
Jovian dust stream [06Pos]	H^+, C^+, Rh^+, Na^+ dominant O^+, Si^+, K^+, S^+, Cl^+ Weak $RhCl^+$, RhS^+, $RhNa^+$ cluster Spectra often triggered by H^+	Sodium chloride main compound Further alkali metal salts likely Minor sulfurous compounds Silicate core possible
Saturnian dust stream [05Kem2]	Faint spectra; C^+, Rh^+ dominant O^+, Si^+ Occasional Na^+, K^+ Weak $RhSi^+$ cluster, H_3O^+, N^+(?) Spectra always triggered by H^+	Siliceous main compound Occasional water ice mantle possible

the dominant particle composition, with some silicate or alkaline constituents [08Pos, 07Hil2].

Stardust: comet Wild 2 dust and interstellar dust. The in-situ analysis of dust at comet Wild 2 by Stardust's CIDA instrument did not yield the high-resolution spectra that the instrument had shown in calibration tests. Nevertheless, it was suggested that complex organic particles dominate the compositions of the particles in the vicinity of comet Wild 2 [04Kis]. En route to the comet Stardust collected and analyzed interstellar dust particles. The CIDA instrument provided the first high mass-resolution spectra of a few tens of presumably interstellar grains. The spectra indicate that the main constituents of interstellar grains are organic with a high oxygen and low nitrogen content. It was suggested that polymers of derivatives of the quinine type are consistent with all impact spectra recorded [04Kru].

4.3.5.3.4.2 Analysis of collected dust particles

Atmospheric collections: interplanetary dust. Extraterrestrial grains (called IDPs, which stands for Interplanetary Dust Particles) are subdivided according to morphology: (1) aggregates, (2) spheres, and (3) particles that are neither a sphere nor an aggregate (Fig. 7) [98Rie, 01Jes]. Other characteristics are chemistry, optical and infrared properties (Table 9). About half of the collected particles have elemental abundances that closely (within a factor 3) match the bulk abundances of CI or CM carbonaceous chondrite meteorites (Table 10). Other extraterrestrial composition groups (Table 11) have been identified by their physical association with chondritic particles.

Particles collected by the NASA program (`http://curator.jsc.nasa.gov/dust/`) are identified in the catalogue by a SEM image, an energy dispersive spectrum (EDS) representing the bulk composition, size, shape, color, porosity and whether the particle is transparent, translucent, or opaque (in visible light).

Aggregate particles consist of sub-micron sized grains that are loosely bound and the particle structure is quite porous. The porosities range from 0 to 90% with a mean of 11%. The densities range from 300 to 4300 kg/m^3 with an average of 2400 kg/m^3 [98Rie]. About 10% of the aggregate particles are spherules that are not porous and do not contain sulfur. The sulfur depletion is probably the result of thermal alteration and the particle shapes imply that the particles were

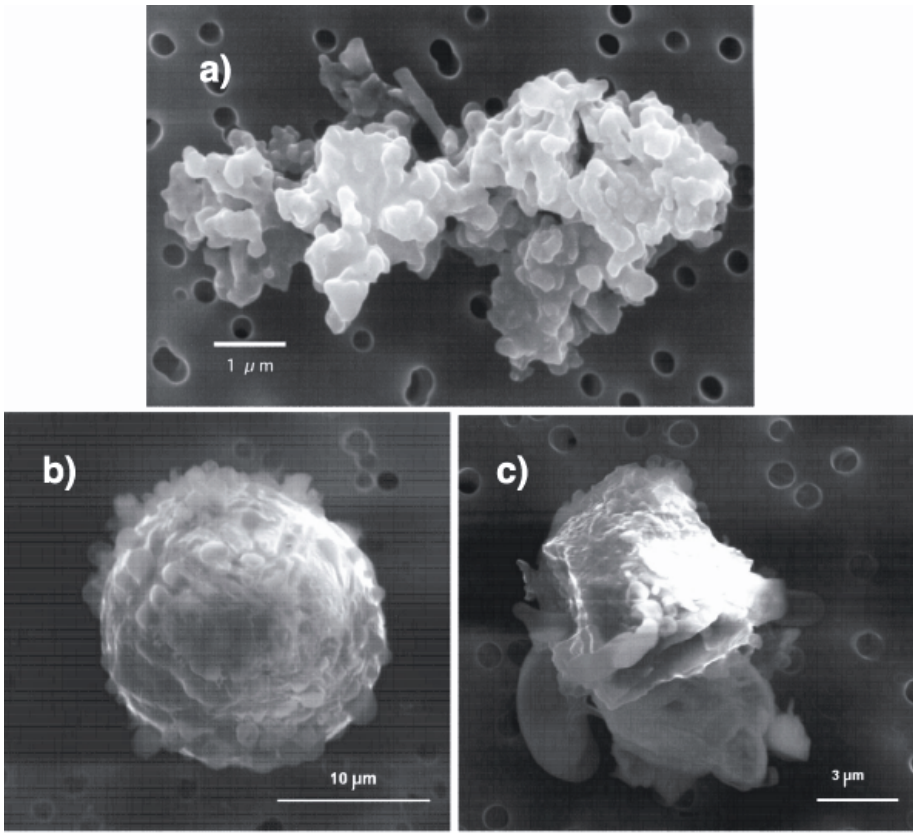

Fig. 7. Interplanetary dust particles collected in the stratosphere (NASA images): a) porous chondritic aggregate particle, b) spherical chondritic particle, and c) irregular non-chondritic particle consisting of single mineral grains or coarse grained assemblages of a few grains.

molten probably during atmospheric entry. The Fe, S and Ni (FSN) particles are roughly similar to meteoritic troilite or pyrrhotite containing a few percent nickel. Large silicate grains are iron poor olivines and pyroxenes with clumps of chondritic aggregates adhering to their surfaces.

The low albedo of typical IDPs is caused by their porous structure and the presence of strongly absorbing material. The absorbing fine-grained matrix material includes carbon, small sulfides and GEMS (sub-micrometer components composed of Glass with Embedded small Metal and Sulfide grains). The abundant nm-sized metal grains in GEMS are the major source of absorption in many of the IDPs [95Bra, 99Bra].

Table 9. Properties of extraterrestrial stratospheric particles [98Rie, 06Bro, 78Bro1, 78Bro2, 78Fly].

	Chondritic particles		Non-chondritic particles	
	Aggregates	Spheres	FSN particles	Silicate particles
Abundance	55%	5%	30%	10%
Optical properties	Black (opaque)	Opaque, some transparent	Opaque	Transparent and opaque
Chemical signature	Chondritic with bulk carbon and sulfur, both > 4 wt.%	Chondritic but no sulfur	S/Fe = 1 to 0 Fe/Ni = ∞ to 10	Fe, Mg-silicates with sulfur
Grain sizes (μm)	0.01 to >1, mostly 0.1 to 0.3	No data	2 to 6	4 to 16
Mineralogical properties	Pyroxene, Olivine, Pyrrhotite, amorphous Fe-Mg-Si-phase	Olivine, Pyroxene, Magnetite	Magnetite, (Ni)-Fe-sulfide	Olivine, Pyroxene, Enstatite, Fe-sulfide

Table 10. Average composition of chondritic aggregate IDPs compared with bulk composition of CI and CM meteorites. Elements are normalized to Si [78Bro1, 81Hud].

	Aggregate IDPs	CI	CM
Mg	0.85	1.06	1.04
Fe	0.63	0.90	0.84
S	0.35	0.46	0.23
Al	0.063	0.085	0.084
Ca	0.048	0.071	0.072
Na	0.049	0.060	0.035
Ni	0.037	0.051	0.046
Cr	0.012	0.913	0.012
Mn	0.015	0.009	0.006
Ti	0.0022	0.002	0.002

Table 11. Large mineral grains in chondritic aggregate IDPs [81Fra].

	Size (μm)	Composition
Olivine	0.2 to 1	Forsterite
Pyroxene	>1	Enstatite
Fe-sulfide	0.2	Pyrrhotite
Low-Ni Fe metal	0.2	Taenite
Fe-carbide	Polycrystalline rim (15 nm)	Cohenite

Stardust: comet Wild-2 dust. In January 2006 the Stardust sample capsule returned safely to Earth with thousands of particles from comet 81P/Wild 2 for laboratory study [06Bro, 06Fly, 06Hor, 06Kel, 06McK, 06Zol]. Impact tracks in aerogel created by particles varying from dense mineral grains to loosely bound, polymineralic aggregates ranging from 0.01 to 100 μm in

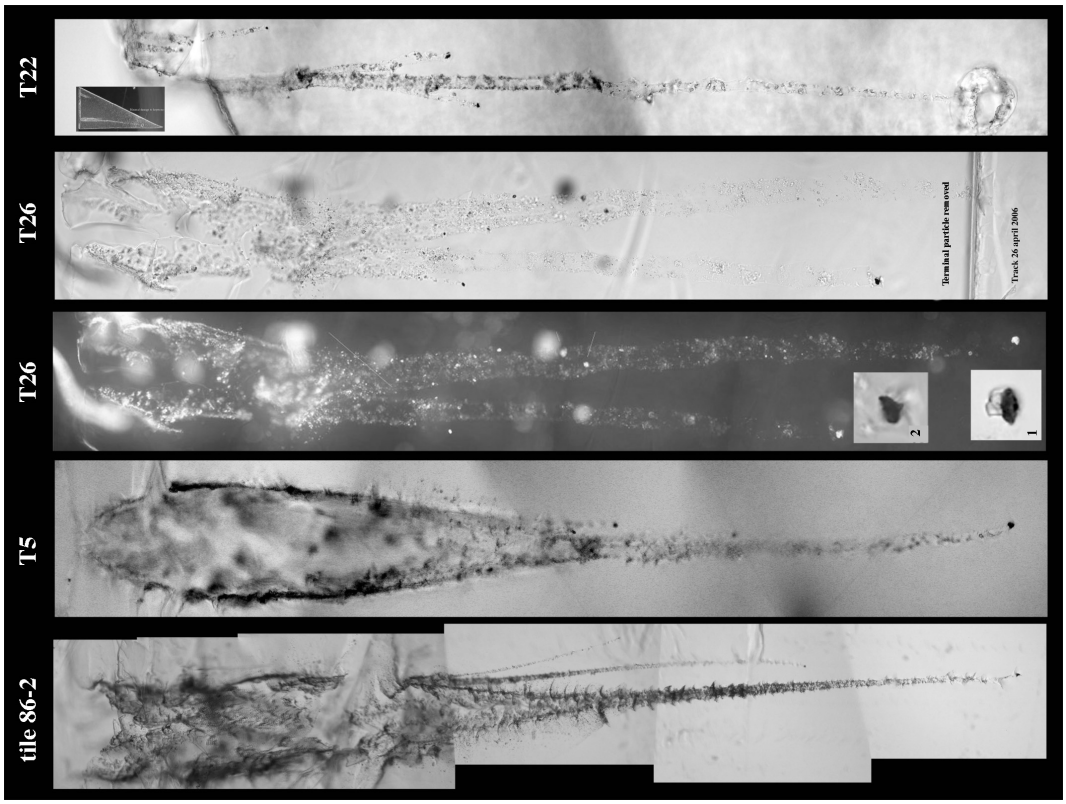

Fig. 8. Tracks in aerogel with particle fragments along the track and in most cases a terminal particle at the end (Stardust Mission, NASA images).

size displayed diverse impact features (Fig. 8). Nonfragmenting particles produced carrot-shaped tracks which contain deeply penetrating grains whereas fragmenting particles produced tracks with bulbous upper regions and sometimes multiple roots. Residues in impact craters in aluminum foil targets were also analyzed.

The particles are chemically heterogeneous; however the mean elemental composition of comet Wild 2 particles is consistent with CI meteorite composition. The particles are weakly constructed mixtures of nanometer-scale grains with occasional much larger Fe-Mg silicates, Fe-Ni sulfides, Fe-Ni metal phases. A very wide range of olivine and low-Ca pyroxene compositions has been found. The organics are rich in oxygen and nitrogen compared with meteoritic organics. Aromatic compounds are present but less abundant than in meteorites and IDPs. The organics found in comet Wild 2 show a heterogeneous and unequilibrated distribution in abundance and composition. Hydrogen, carbon, nitrogen, and oxygen isotopic compositions are heterogeneous among particle fragments; however, extreme isotopic anomalies are rare, indicating that the comet is not a pristine aggregate of presolar materials. A single particle has been found with a ratio $^{17}O/^{16}O = 10^{-3}$ which is a factor 2.6 higher than the Solar System value and is similar to that of some presolar grains found in meteorites. The abundance of high-temperature minerals such as forsterite and enstatite appears to have formed in the hot inner regions of the solar nebula.

4.3.5.3.5 Flux measurements in the interplanetary dust cloud

Many spacecraft with in-situ dust detectors have flown far away from the Earth and measured meteoroid fluxes in deep space (Table 1). Helios 1 was orbiting the Sun with perihelion at 0.3 AU and aphelion at 1 AU. It was equipped with two detectors, directed to the ecliptic south pole and ecliptic plane, respectively. On their grand tour to the outer Solar System, Pioneers 10 and 11 carried penetration detectors mounted on the rear side of its high-gain antenna, that normally pointed to Earth. These detectors were operational up to 18 AU from the Sun. Ulysses had an impact ionisation detector attached to the spinning spacecraft with a mounting angle close to 90°. Ulysses was launched to Jupiter, where it made a gravitational manoeuvre to get on an orbit nearly perpendicular to the ecliptic plane, with perihelion at 1.3 AU and aphelion at about 5 AU. Altogether, these four spacecraft have traversed the Solar System on complementary paths and their measurement results are highlighted below.

The Helios 1 spacecraft [80Gru] explored the meteoroid environment deep inside the Earth orbit, down to 0.3 AU from the Sun. It had two dust detectors with relatively small exposed area of several dozen cm^2. However, the number density and orbital velocities of meteoroids close to the Sun are higher, thus their fluxes are significantly higher than near Earth. A long exposure time (the detectors remained operational for about six years) had provided an opportunity to accumulate a statistically significant record of impacts. Note that the Helios detectors were also mass spectrometers determining chemical composition of dust particles. Although directional information on impacts is available, as the spacecraft orientation is known for every impact allowing one to constrain the orbits from which the impactor arrived, we summarize the measurements by Helios 1 in the form of spin-averaged fluxes, thus emphasizing the radial trend (Fig. 9).

The Pioneer 11 spacecraft carried a dust detector composed of a large number of cells with pressurised gas [80Hum]. The cell walls were made of thin foil penetrated by meteoroids with a sufficient mass or velocity. Gas pressure drop caused by leakage was detected electrically. In order to avoid multiple registrations of the same event, the impact counter was turned off for 80 minutes after each event. Penetrated cells were permanently lost. Although no individual cell tracking was implemented, all cells were divided into two groups, or "channels", for the sake of redundancy. Surprisingly, the channels measured tremendously different fluxes. One of the channels of an analogous dust detector on board Pioneer 10 did not function at all. It was suggested that some

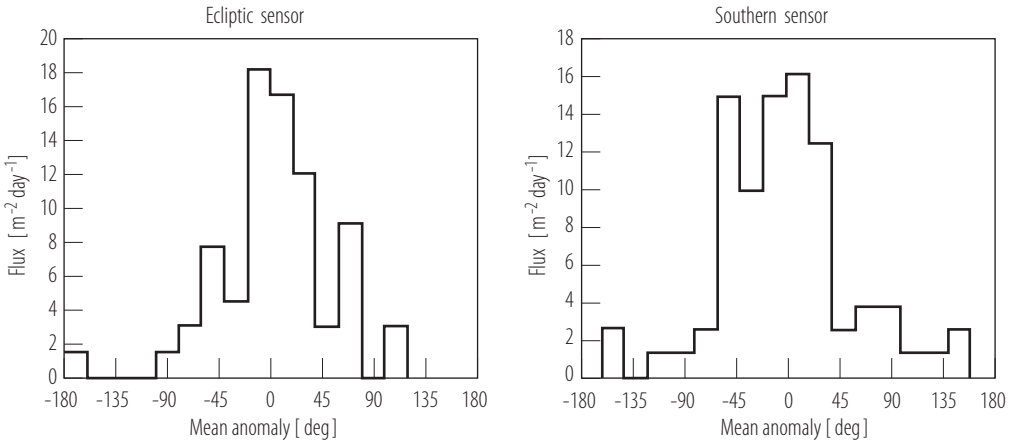

Fig. 9. Spin-averaged meteoroid fluxes on the ecliptic and southern dust detectors installed on Helios 1. The spacecraft was orbiting the Sun in the ecliptic plane, with the perihelion distance at 0.3 AU and aphelion distance at 1 AU. The horizontal axis shows the mean anomaly of the spacecraft (measured from the perihelion). Impacts correspond to a lower mass limit of 3×10^{-12} g at impact speed of 20 km s^{-1}.

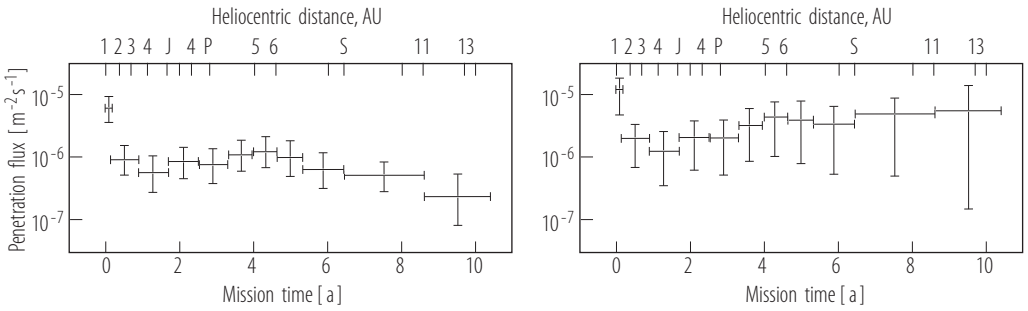

Fig. 10. Meteoroid fluxes on the Pioneer 11 dust detector which was sent to the outer Solar System, flew by Jupiter (label 'J'), returned for a short time in the inner Solar System along a new hyperbolic orbit (label 'P' marks the last perihelion passage) and headed for Saturn (label 'S'). Left: the fluxes originally derived [80Hum] assuming that the detector was fully functional. Right: the fluxes derived [02Dik] taking into account the possibility of a partial damage of the detector cells at the spacecraft launch. In both cases, the meteoroid fluxes decrease considerably between Earth and the asteroid belt and then stabilize. In the second case, the uncertainty of flux determination grows with time as the sensitive area of the damaged instrument decreases, with an unknown number of disabled cells. The cell walls were penetrated by meteoroids bigger than about 6×10^{-9} g at an impact speed of 20 km s^{-1}.

cells of these dust detectors could be damaged at launch [02Dik]. Since the exact number of destroyed cells is impossible to recover, a probabilistic model of the instrument was constructed and applied to re-derive the true fluxes.

Fig. 10 shows the penetration fluxes both for the original assumption that the detector was intact and based on the probabilistic model of a partially damaged detector. Both approaches provide similar fluxes near Earth, including a sharp decrease of the number of meteoroids with heliocentric distance, up to the asteroid belt. Further away from the Sun, a flattening of the flux is also a consensus. As the cells were spent in impact events, and the number of active cells decreased and approached the unknown number of cells destroyed at launch, the uncertainty of flux measurements in the probabilistic model of the instrument naturally increased. While the original approach suggests that the fluxes may have continued to decrease near and after Saturn fly-by, the more realistic model of the measurements allows for a continued flat or even rising trend.

The Ulysses spacecraft was sent into a very unique orbit nearly perpendicular to the ecliptic plane [92Gru2]. As it was expected from the visual and infrared observations, the number density of meteoroids decreases away from that plane. Several ecliptic plane crossings were especially interesting to measure the vertical density profile of the meteoroid cloud in-situ. The Ulysses spacecraft was spin-stabilized, with a rotation period of about 12 s. The rotation angle of the spacecraft was measured from its northern ecliptic culmination. It was stored for each impact. Figure 11 shows a color map of meteoroid fluxes versus time and rotation angle. Most of the impacts near 90° are in fact due to the interstellar dust. Its flux is little changing up to 2000, independent on spacecraft position with respect to the ecliptic plane. Since 2000, it shows a decrease due to depletion of interstellar dust in the Solar System due to the Solar cycle and the corresponding interplanetary magnetic field change. The ecliptic plane crossings are marked by rises of interplanetary dust fluxes from the north (perihelion northward crossings in 1995 and 2001) and south (aphelion southward crossings in 1992, 1998 and 2004).

4.3.5.3.6 Solar System dust streams

The dust experiments on the solar orbiting Pioneer 8 and 9 spacecraft recorded a flux of sub-micron sized dust grains ($\sim 2 \times 10^{-4}$ m^{-2} s^{-1}) arriving from the solar direction [73Ber, 75McD].

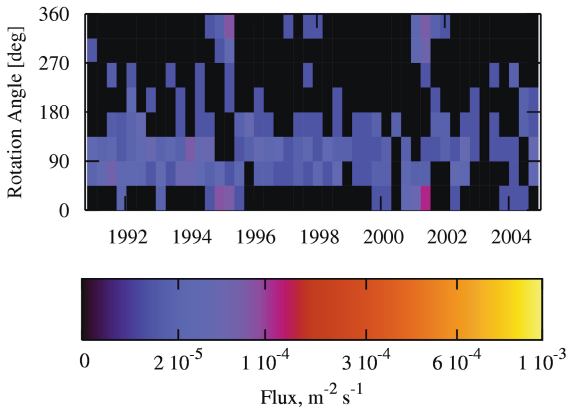

Fig. 11. (see color-picture part, page 626) Meteoroid fluxes measured by the Ulysses dust detector, as a function of mission time and detector orientation [97Gru, 06Kru2]. The rotation angle is the azimuth of the detector pointing axis measured from its ecliptic northern culmination. Selected are impacts by meteoroids bigger than $\sim 10^{-13}$ g at the velocity of 20 km s^{-1}.

It was concluded that these particles move on hyperbolic orbits that leave the Solar System. Zook and Berg [75Zoo2] called these particles beta-meteoroids and deduced that they were probably primarily generated as debris resulting from mutual collisions between larger meteoroids and were driven out of the Solar System by solar radiation pressure [75Zoo1]. Measurements by the Helios spaceprobe [80Gru] and the HITEN satellite [01Gru2, 96Sve] supported these observations in the ecliptic plane. Observations by Ulysses found this small particle stream also over the poles of the Sun [95Bag2, 99Weh, 04Weh]. These observations are interpreted to be due to beta-meteoroids affected by the solar wind magnetic field [96Ham].

In interplanetary space within 3 AU from Jupiter Ulysses observed a high flux (up to 0.1 m^{-2} s^{-1}) of tiny particles emanating from the Jovian system [93Gru, 93Bag]. This flux was modulated with a period of 28 ± 3 days. It was immediately recognized that Jupiter's magnetosphere would eject submicron sized charged dust particles [93Hor1, 93Ham]. Analyzing the Ulysses data Zook et al. [96Zoo] concluded that the streams consist of a few nanometer sized grains that interact strongly with the solar wind magnetic field. Twelve years later, during Ulysses second approach to Jupiter dust streams were observed anew [06Kru3, 05Kru2]. On approach to Jupiter measurements by Galileo confirmed the Ulysses observations [96Gru1, 96Gru2]. Later while Galileo was in orbit about Jupiter dust stream particles were characterized within Jupiter's magnetosphere [98Gru, 03Kru1, 03Kru2, 05Kru1]. The measurements showed strong flux fluctuation with Jupiter's 10-hour rotation period which demonstrated the electromagnetic interaction of the dust grains with the ambient magnetic field of Jupiter. Frequency analysis of the observed impact rate showed an additional strong peak at 42 h - the orbital period of Io [00Gra]. This confirmed that tiny dust particles were released into the magnetosphere from the volcanic plumes on Io and ejected out of the Jovian system by Jupiter's giant magnetic field. During its fly-by of Jupiter the Cassini dust analyzer recorded the Jupiter dust streams again and analyzed the composition of the particles [06Pos]. Also in Saturn's environment tiny dust stream particles were recorded by Cassini emanating from the ring system [05Kem2, 05Kem1]. All these dust stream particles will eventually end up as interstellar dust.

4.3.5.3.7 Interstellar dust in the heliosphere

In 1992, after its Jupiter flyby, the Ulysses spacecraft positively identified interstellar dust penetrating deep into the Solar System. It detected impacts predominantly from a direction that was

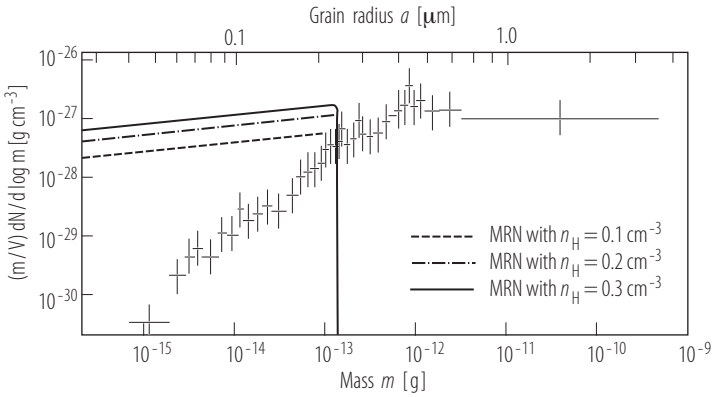

Fig. 12. Mass distribution of interstellar grains inside the heliosphere [99Fri]. The dashed lines show the mass density for three different densities of hydrogen atoms in the local interstellar medium [77Mat]. The top axis gives the grain radius corresponding to the mass shown on the bottom axis for spherical silicate grains.

opposite to the expected impact direction of interplanetary dust grains (Fig. 11). On average, the impact velocities exceeded the local Solar System escape velocity [94Gru]. The motion of the interstellar grains through the Solar System was approximately parallel to the flow of neutral interstellar hydrogen and helium gas, both traveling at a speed of 26 km/s [95Bag1]. The interstellar dust flow persisted at higher latitudes above the ecliptic plane, even over the poles of the Sun, whereas interplanetary dust was strongly depleted away from the ecliptic plane [97Gru].

Ulysses measured the interstellar dust stream at high ecliptic latitudes between 2 and 5 AU. The masses of interstellar grains range from 10^{-18} kg to about 10^{-13} kg with a maximum at about 10^{-16} kg [00Lan]. In Fig. 12 the interstellar dust mass density observed by Ulysses during 1992 and 1996 is compared with the mass densities in the local interstellar medium, assuming a gas-to-dust mass ratio of 100 [99Fri, 77Mat]. The total interstellar dust mass flux is about 10^{-19} kg/s m^2. The in-situ dust detectors on board Cassini, Galileo and Helios, [06Alt, 03Alt, 05Alt] detected interstellar dust in heliocentric distance range between 0.3 and 3 AU in the ecliptic plane. There were significant differences in the particle sizes that were recorded at different heliocentric distances. Small ($< 3 \cdot 10^{-16}$ kg) interstellar grains were only detected outside 3 AU heliocentric distance [00Lan]. In the distance range between 0.7 and 3 AU interstellar particles were bigger than 10^{-15} kg. The limiting masses increased to ca. 10^{-14} kg at 0.3 AU. The interstellar dust stream is strongly filtered by solar radiation pressure. Interstellar particles with optical properties of astronomical silicates or organic refractory materials are consistent with the observed radiation pressure effects [99Lan].

Ulysses has monitored the interstellar dust flow through the Solar System for more than 16 years (Fig. 13) covering more than 2/3 of a complete 22-year solar cycle. In mid 1996, the interstellar dust flux decreased by a factor 3. This flux modulation is attributed to the filtering of small grains by the solar wind magnetic field during solar minimum conditions [00Lan, 98Lan, 03Lan, 00Man, 03Cze]. Until early 2005 the upwind direction of the interstellar grains was within a few 10 degrees in agreement with the interstellar helium flow direction [98Lan, 99Fri, 07Kru]. Six years later, when Ulysses was travelling through almost the same spatial region and had an almost identical detection geometry for interstellar grains, the upwind direction of the grains was somewhat wider and shifted by about 30 degrees away from the helium flow direction towards southern ecliptic latitudes [07Kru].

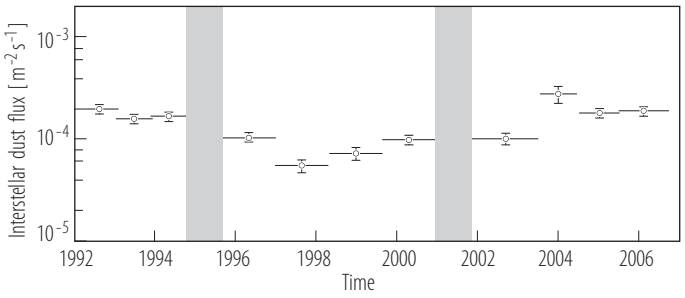

Fig. 13. Interstellar dust flux measured by Ulysses [07Kru]. The dashed regions in 1995 and 2001 show the periods of Ulysses perihelion passages where the distinction of interstellar dust from interplanetary impactors is difficult. In 2003 and 2004 a possible contamination by jovian dust stream particles around Jupiter flyby, which occurred in February 2004, may lead to an erroneously enhanced interstellar flux (Figure courtesy of Markus Landgraf).

4.3.5.4 Theory

4.3.5.4.1 Sources

Dust particles cannot grow by coagulation in the interplanetary space at the present epoch. In the early days of the Solar System, when the Sun was surrounded by a gas disk, gas drag reduced the relative velocities of dust particles and allowed them to stick in soft collisions. Then these particles continued to grow to planetesimals, and the 100-km sized protoplanets accelerated their growth through the gravitational attraction. As the giant planets were formed, they scattered gravitationally some of the planetesimals into very distant orbits, forming the trans-neptunian belt extending from about 30 to 100 AU near the Laplace plane of the Solar System, and the Oort cloud, a spherical halo of planetesimals stretching up to 10,000 AU, where the solar gravity becomes negligible with respect to that of the Galaxy. A number of planetesimals in the inner Solar System were prevented from forming a planet by the gravitational perturbations due to rapidly growing Jupiter, they rest in the asteroid belt. Some comets migrated to the asteroid belt too.

In the present epoch, gas is rather thin in the Solar System and it cannot damp relative velocities. Dust particles are destroyed in collisions at several to several tens km/s speeds. Therefore, they should be continuously replenished. The main source of dust particles today is the destruction or erosion of the planetesimals left from the formation of the Solar System. They are comets and asteroids. Being mostly solid bodies without volatile materials, asteroids generate dust in mutual collisions leading to cascade collisions of the released boulders and meteoroids.

Comets contain a significant fraction of water and gases that are frozen far from the Sun and sublimated at higher temperatures close to it. Gas streams elevate dust particles embedded in ice from comet surfaces. Collisions between comets and asteroids have also been quoted as a possible origin of meteoroid streams [50Whi]. Destruction of the stream meteoroid produces dust particles, colliding bigger dust particles produce smaller dust particles.

Volcanoes on planetary satellites (Io, Enceladus) can send meteoroids or dust particles to space [06Spa].

4.3.5.4.2 Dynamics

The Solar gravity dominates the dust particle dynamics from μm size and above. The particle motion on short time scales can well be approximated by a Keplerian orbit around the central star. For dust grains less then several hundred μm in size, the effective solar mass has to be calculated, taking into account the reduction of the gravitational pull by the direct solar radiation pressure

acting in the opposite direction. As both forces are inversely proportional to the square distance from the Sun, a dimensionless ratio $\beta = Q_{\rm pr}L_\odot/(GM_\odot)$ is useful, where $Q_{\rm pr}$ is the radiation pressure efficiency factor (depends on particle material and shape), $L_\odot$ is the solar luminosity and $GM_\odot$ is the solar gravitational parameter. When the β ratio is below unity, the particle orbit is bound, otherwise it is a parabolic or hyperbolic path away from the Solar System. All particles in space are charged by the photo-effect from solar UV radiation and by the interaction with the ambient plasma. Small particles ($< 0.1\mu$m) interact strongly with the solar wind magnetic field.

When a new dust particle is created – through collisional destruction of a bigger particle or through emission by a comet – its orbit can instantaneously become different from the parent object due to the reduced effective solar mass. The semimajor axis a and eccentricity e of the orbit of the grain released at the distance r from the Sun are related to the parent body orbit elements (subscript p) via

$$a = a_{\rm p}\left(\frac{1-\beta}{1-2a_{\rm p}\beta/r}\right), \qquad e = \left|1 - \frac{(1-2a_{\rm p}\beta/r)(1-e_{\rm p}^2)}{(1-\beta)^2}\right|^{1/2} \tag{1}$$

The particles are typically created in clusters, having slightly different ejection velocities and therefore slightly different semimajor axes. The rate of the orbital motion depends on semimajor axis, thus the particle cluster is elongated over time, eventually its members are distributed uniformly over the mean anomaly.

If the particle stays in the Solar System, the action of weaker forces becomes important. Planetary gravity perturbs the Keplerian orbits of dust particles. In most frequent cases, the action of a planet can be approximated by the effect of its mass distributed uniformly along the planet's orbit. It causes precession of the orbital node and perihelion of the dust particle. Precession rates depend on the separation from the planet, the orbital nodes and perihelia of dust clouds become uniformely distributed over time.

Near a planet, where its gravity exceeds that of the Sun, an interplanetary particle moves approximately along a hyperbolic orbit about the planet. The outcome of such motion for its heliocentric orbit is a nearly instantaneous (days vs. years of the orbital period) rotation of its planetocentric velocity vector. When the rotation angle is long then the heliocentric orbit change is significant. The particle can even get on a hyperbolic heliocentric trajectory. After a close encounter, only the Tisserand quantity $T = a_0/a + 2\sqrt{(1-e^2)a/a_0}\cos i$ is approximately conserved, the rest of the elements can change sharply. Here i is the inclination of the particle orbit off the planet's orbital plane, a_0 is the radius of the planetary orbit.

When the particle orbital period is in a simple ratio with that of the planet, the particle can be trapped in a mean-motion resonance. Spatial structures can be created in this case like clouds of enhanced density in the vicinities of the triangular Lagrangian points on the planet orbit. Secular resonances occur when the orbital node or perihelion precession periods are in a simple ratio with that of a planet.

The particles from ~ 1 to $\sim 100\mu$m in size are significantly affected by the Poynting-Robertson effect, a component of radiation pressure tangential to the grain's motion. The effect is associated with aberration of light, i.e. an apparent displacement of the Sun due to the particle motion. The effect leads to a secular loss of angular momentum, the grain orbit is circularized and its semimajor axis undergoes a gradual decrease. The Poynting-Robertson effect can drag the particles in and out of resonances, which results in non-linear dynamics changing particle orbits in non-trivial ways, e.g. raising or damping the orbit eccentricities and inclinations.

An effect similar to the Poynting-Robertson drag is caused by the solar wind, except that the corpuscular matter emitted by the Sun is significantly slower than the speed of light (400 km/s versus 3×10^5 km/s). The aberration angle is, therefore, longer but the momentum carried by wind is considerably smaller than that of the solar radiation. The solar wind drag is often approximated by adding a 30% correction factor to the Poynting-Robertson drag.

Many dust particles in the Solar System are essentially in collective dynamics through collisional interaction. Usually destructive, the collisions are described by a Boltzmann-type continuity equation with an integral term. Collisions remove big dust particles and meteoroids and generate small dust grains.

Non-destructive collisions may lead to dust drag – orbital change of a big particle by an anisotropic influx of tiny ones. The dust drag has been reported [05Tri].

The finest dust in the < 100 nm size range is subject to the Lorentz force. The magnetic fields of the Sun and giant planets strongly affect the motion of such particles generated through collisions or evaporation, or ejected from satellites like Io, their trajectories are not Keplerian. These particles are eventually carried out of the Solar System by the solar wind magnetic field.

4.3.5.4.3 Sinks

There is a number of processes that limit the lifetimes of dust particles in the interplanetary space.

Mutual collisions at a few to a few tens km/s grind the particles down to smaller sizes. This is especially important for meteoroids above ~ 100 μm in size.

The Poynting-Robertson effect drives smaller dust particles down to the Sun. As they approach close to the star, they begin to evaporate. At a temperature of ~ 300 K near Earth and with the distance R dependence of the temperature $\propto R^{-1/2}$, the particle temperatures reach 3000 K at 0.01 AU, or 1.5×10^6 m away from the center of the Sun. Few materials can survive such heat intact. Dust particles can also break up due to the thermal heat, with the fragments being either sufficiently small to take hyperbolic paths away from the Solar System (due to their $\beta > 1$) or disrupting and evaporating further.

Gravitational scattering by giant planets can eject dust particles from the Sun, whereas the particles hitting planets are accreted.

4.3.5.4.4 Populations

Combining the knowledge of sources, dynamics and sinks, a steady-state model of the orbital distributions of interplanetary dust can be constructed. A number of the above-listed processes have been taken into account when the most recent ESA meteoroid model was designed [05Dik]. It can be used to illustrate the large-scale structure of the interplanetary dust cloud up to 5-10 AU.

The mass distribution of the model was based on the flux at 1 AU [85Gru]. However, since big meteoroid-sized particles (mass $m > 10^{-5}$ g) and small dust grains ($m < 10^{-5}$ g) have different dynamics, the two corresponding mass ranges were separated. They are normalized to unity at $m = 10^{-12}$ g in Fig. 14.

In each mass range, the rate of the orbital evolution depends mainly on size, while the topology of particle trajectories is nearly mass-independent, at least on the large scale. Figure 15 shows the three-dimensional distributions of particle orbits $f(a, e, i)$ from the ESA model, integrated either over all inclinations (left column) or eccentricities (right column). The upper row of panels (plots A and E) shows the distributions of big particles from asteroids. Their lifetimes are limited to the collisional lifetimes with more abundant smaller grains, and they cannot drift away from their parent bodies over their short lifetimes. In the second row (plots B and F), the distributions of small grains from asteroids spiraling toward the Sun under the Poynting-Robertson effect are shown. It is seen that the Poynting-Robertson drag circularizes particle orbits over time yet leaves the inclinations intact. In reality, resonances with planets (Jupiter and Earth) disperse the inclinations somewhat [98Kor].

The bottom half of Fig. 15 displays the distributions of particles from comets in Jupiter-crossing orbits. Note that in the model [05Dik], these distributions are fitted to the dust measurements rather than to rather poorly constrained dust production rates by comets. Plots C and G display

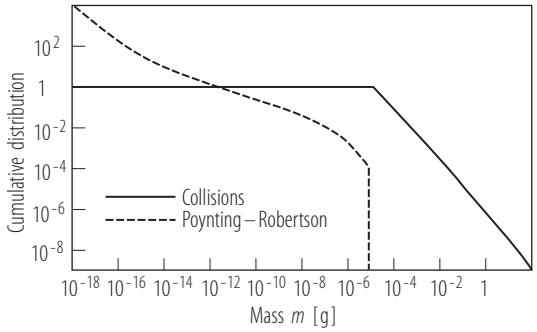

Fig. 14. Cumulative mass distributions of interplanetary dust particles in the ESA meteoroid model [05Dik], normalized to unity at 10^{-12} g. Either collisions or the Poynting-Robertson drag determine the particle lifetimes in each mass range. Since collision rates and Poynting-Robertson drag rate have different dependence on size, the distributions in two mass ranges have different slopes.

the big particle distributions. They are entirely governed by gravitational scattering by Jupiter and are naturally confined to the region of gravitational encounters. Only collisions or ejection from the Solar System can remove them. Small dust grains plotted in the bottom row (D and H) can leak from the region of encounters driven by the Poynting-Robertson effect. Their dynamics are still governed by encounters with Jupiter if they cross its orbit. The scattering time for them is much shorter than the Poynting-Robertson time at that long distance from the Sun.

Acknowledgements. Helpful comments and support in the preparation of the manuscript were provided by Harald Krüger, Frank Postberg, and Uwe Beckmann.

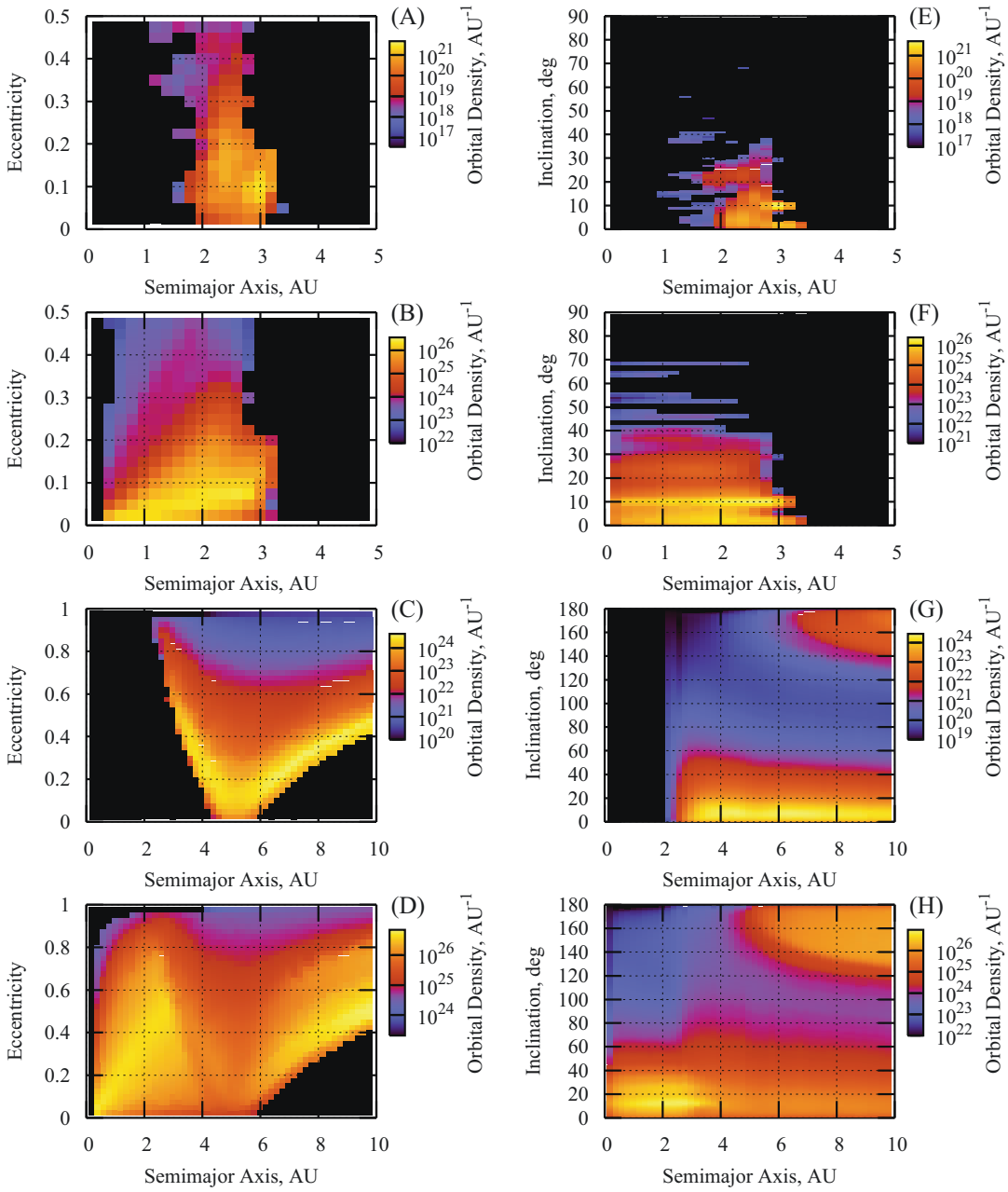

Fig. 15. (see color-picture part, page 627) Orbital distributions of interplanetary dust particles in the ESA meteoroid model [05Dik], calculated for the minimum mass threshold 10^{-12} g. They can be multiplied by the mass distributions in Fig. 14 to obtain the absolute numbers of particles above any other mass covered by the model. The left column shows the distribution in semimajor axis and eccentricity, the right column shows the distribution in semimajor axis and inclination. Four distinct populations are shown. Plots A and E: the big dust particles ($m > 10^{-5}$ g) from asteroids in collisional regime. Plots C and G are the same for comets in Jupiter-crossing orbits. Plots B and F: small dust grains (mass $m < 10^{-5}$ g) from asteroids, spiraling toward the Sun under the Poynting-Robertson effect. Plots D and H are the same for comets.

4.3.5.5 References for 4.3.5

50Whi Whipple, F.L., Hamid, S. E.-D.: On the origin of the Taurid meteors. Astrophys. J. **55** (1950) 185.

51Opi Öpik, E.J.: Collision probabilities with the Planets. Proc. Roy. Irish Acad. **A54** (1951) 165-172.

69Ber Berg, O.E., and Richardson, F.F.: The Pioneer 8 cosmic dust experiment. Rev. Sci. Instrum. **40** (1969) 1333-1337.

72Coo Cook, A.E., Flannery, M.R., Levy, H., McCrosky, R.E., Sekanina, Z., Shao, C.-Y., Southworth, R.B., Williams, J.T.: Meteor Research Program. Cambridge, MA: NASA CR-2109, Smithsonian Institution, 1972.

73Ber Berg, O.E.; Grün, E.: Evidence of hyperbolic cosmic dust particles. Space Research XIII, **2** (1973) 1047-1055.

73Die Dietzel, H., Eichhorn, G., Fechtig, H., Grün, E., Hoffmann, H.J., Kissel, J.: The HEOS A-2 and Helios micrometeoroid experiments. J. Phys. E: Sci. Instrum. **6** (1973) 209-217.

73Sou Southworth, R.B., and Sekanina, Z.: Physical and dynamical studies of meteors. NASA CR-2316, Smithsonian Institution, Cambridge, MA, 1973.

75Hor Hörz, F., Brownlee, D.E., Fechtig, H., Hartung, J.B., Morrison, D.A., Neukum, G., Schneider, E., Vedder, J.F., Gault, D.E.: Lunar microcraters: Implications for the micrometeoroid complex. Planet. Space Sci. **23** (1975) 151-172.

75McD McDonnell, J.A.M., Berg, O.E., Richardson, F.F.: Spatial and time variations of the interplanetary microparticle flux analysed. Planetary and Space Science **23** (1975) 205-214.

75Sek Sekanina, Z., Southworth, R.B.: Physical and dynamical studies of meteors. Meteor-fragmentation and stream-distribution studies, Final Report Smithsonian Astrophysical Observatory, Cambridge, MA., Publication Date: 11/1975

75Zoo1 Zook, H.A.: Hyperbolic cosmic dust - Its origin and its astrophysical significance. Planetary and Space Science **23** (1975) 1391-1397.

75Zoo2 Zook, H.A., Berg, O.E.: A source for hyperbolic cosmic dust particles. Planetary and Space Science, **23** (1975) 183-203.

76Han Hanner, M.S., Sparrow, J.G., Weinberg, J.L., Beeson, D.E.: Pioneer 10 observations of zodiacal light brightness near the ecliptic: Changes with heliocentric distance, In: Lecture Notes in Physics, 48: Interplanetary Dust and Zodiacal Light (H. Elsasser and H. Fechtig (Eds.)) Springer-Verlag, New York, 29-35, 1976.

77Bro1 Brownlee D.E., Rajan R.S., Tomandl D.A.: A chemicaland textural comparison between carbonaceous chondrites and interplanetary dust, in: Comets, Asteroids, Meteorites - Interrelations, Evolutions and Origins, A.H. Delsemme ed., Univ. of Toledo, TRoledo, 137-141, 1977.

77Bro2 Brownlee D.E., Tomandle D.A., Olszewski E.: Interplanetary dust: A new source of extraterrestrial material for laboratory studies. Proc. Lunar Sci. Conf. **8** (1977) 149-160.

77Dal Dalmann, B.-K., Grün, E., Kissel, J., Dietzel, H.: The ion-composition of the plasma produced by impacts of fast dust particles, Planetary and Space Science **25** (1977) 135-147.

77Mat Mathis, J.S., Rumpl, W., Nordsieck, K.H.: The size distribution of interstellar grains. Astrophysical Journal **280** (1977) 425-433.

78Bro1 Brownlee D.E.: Interplanetary dust: Possible implications for comets and presolar interstellar grains, in Protostars and Planets, T. Gehrels, ed., Arizona press, Tucson, 134-150, 1978.

78Bro2 Brownlee D.E.: Microparticle studies by sampling techniques, in: Cismic Dust, J.A.M. McDonnell ed., Wiley Interscience, New York, 295-336, 1978.

78Dum Dumont, R., Levasseur-Regourd, A.C.: Zodiacal light photopolarimetry. IV - Annual variations of brightness and the symmetry plane of the zodiacal cloud: Absence of solar-cycle variations. Astron. Astrophys. **64** (1978) 9-16.

78Fly Flynn, G.J., Fraundorf, P., Shirck, J., Walker, R.M.: Chemical and structural studies of 'Brownlee' particles, In: Lunar and Planetary Science Conference, 9, Vol. 1, Pergamon Press, Inc., New York, 1187-1208, 1978.

80Gru Grün, E., Pailer, N., Fechtig, H., Kissel, J., Orbital and physical characteristics of micrometeoroids in the inner Solar System as observed by HELIOS 1. Planetary and Space Science **28** (1980) 333-349.

80Hum Humes, D.H.: Results of Pioneer 10 and 11 meteoroid experiments - Interplanetary and near-Saturn. Journal of Geophysical Research **85** (1980) 5841-5852.

80Lev Levasseur-Regourd, A.C., Dumont, R.: Absolute photometry of zodiacal light. Astron. Astrophys. **84** (1980) 277-279.

80Pai Pailer, N., Grün, E.: The penetration limit of thin films. Planetary and Space Science **28** (1980) 321-325, 327-331.

81Fra Fraundorf P.: Interplanetary dust in the transmission electron microscope: diverse materials from the early Solar System. Geochim. Cosmochim Acta **45** (1981) 916-976.

81Gru Grün, E.: Physikalische und Chemische Eigenschaften des interplanetaren Staubes – Messungen des Mikrometeoritenexperimentes auf Helios, Forschungsbericht, BMFT W 81-034, 194 pages, 1981.

81Hud Hudson, B., Flynn, G. J., Fraundorf, P., Hohenberg, C.M., Shirck, J.: Noble Gases in Stratospheric Dust Particles: Confirmation of Extraterrestrial Origin. Science **211** (1981) 383-386.

84Der Dermott, S.F., Nicholson, P.D., Burns, J.A., Houck, J.R.: Origin of the Solar System dust bands discovered by IRAS.em Nature **312** (1984) 505-509.

84Eas East, I.R., Reay, N.K.: The motion of interplanetary dust particles. I - Radial velocity measurements on Fraunhofer line profiles in the Zodiacal Light spectrum. Astron. Astrophys. **139** (1984) 512-516.

84Hau Hauser, M.G., Gillett, F.C., Low, F.J., Gautier, T.N., Beichman, C.A., Aumann, H.H., Neugebauer, G., Baud, B., Boggess, N., Emerson, J.P.: IRAS observations of the diffuse infrared background. Astrophysical Journal Letters **278** (1984) L15-L18.

84Low Low, F.J., Young, E., Beintema, D.A., Gautier, T.N., Beichman, C.A., Aumann, H.H., Gillett, F.C., Neugebauer, G., Boggess, N., Emerson, J.P.: Infrared cirrus - New components of the extended infrared emission. Astrophys. J. Lett. **278** (1984) L19-L22.

85Dum Dumont, R., Levasseur-Regourd, A.Ch.: Zodiacal light gathered along the line of sight. Retrieval of the local scattering coefficient from photometric surveys of the ecliptic plane, Planet. Space Sci. **33** (1985) 1-9.

85Gie Giese R.H., Lamy P. (eds.): Properties and Interactions of interplanetary Dust, Reidel publishing, Dordrecht, 1985.

85Gru Grün, E., Zook, H.A., Fechtig, H., Giese, R.H.: Collisional balance of the meteoritic complex. Icarus **62** (1985) 244-272.

85Per Perkins, M.A., Simpson, J.A., Tuzzolino, A.J.: A cometary and interplanetary dust experiment on the Vega spacecraft missions to Halley's Comet. Nucl. Instrum. Methods Phys. Res., Sect. A **A239(2)** (1985) 310-323.

85Sag Sagdeev, R.Z., Pellat, R., Sabo, F., et al.: Venus-Halley Mission, Balebanov, V.M., Skuridin, G.A., Vorontzova, E.V., Bassolo, V.S. (eds.), Imprimerie Louis-Jean, Gap., 1985.

85Sim Simpson, J.A., Tuzzolino, A.J.: Polarized polymer films as electronic pulse detectors of cosmic dust particles. Nucl. Instr. and Meth. **A236** (1985) 187-202.

86Kis1 Kissel, J.: The Giotto particulate impact analyzer. ESA Spec. Publ. ESA SP-1077 (1986) 67-83.

86Kis2 Kissel, J., Brownlee, D.E., Büchler, K., Clark, B.C., Fechtig, H., Grün, E., Hornung, K., Igenbergs, E.B., Jessberger, E.K., Krueger, F.R., Kuczera, H., McDonnell, J. A.M., Morfill, G.M., Rahe, J., Schwehm, G.H., Sekanina, Z., Utterback, N.G., Völk, H.J., and Zook, H.A.: Composition of comet Halley dust particles from Giotto observations. Nature **321** (1986) 336-338.

86Kis3 Kissel, J., Sagdeev, R.Z., Bertaux, J.L., Angarov, V.N., Audouze, J., Blamont, J.E., Büchler, K., Evlanov, E.N., Fechtig, H., Fomenkova, M.N., von Hoerner, H., Inogamov, N.A., Khromov, V.N., Knabe, W., Krueger, F.R., Langevin, Y., Leonas, V.B., Levasseur-Regourd, A.C., Managadze, G.G., Podkolzin, S.N., Shapiro, V.D., Tabaldyev, S.R., and Zubkov, B.V.: Composition of comet Halley dust particles from Vega observations. Nature **321** (1986) 280-282.

86McD McDonnell, J.A.M., Alexander, W.M., Burton, W.M., Bussoletti, E., Clark, D.H., Evans, G.C., Evans, S.T., Firth, J.G., Grard, R.J.L., Grün, E., Hanner, M.S., Hughes, D.W., Igenbergs, E., Kuczera, H., Lindblad, B.A., Mandeville, J.-C., Minafra, A., Reading, D., Ridgeley, A., Schwehm, G.H., Stevenson, T.J., Sekanina, Z., Turner, R.F., Wallis, M.K., Zarnecki, J.C.: The Giotto Dust Impact Detection System, ESA Spec. Publ., ESA SP-1077 (1986) 85-107.

86Syk Sykes, M.V., Lebofsky, L.A., Hunten, D.M., Low, F.: The discovery of dust trails in the orbits of periodic comets. Science **232** (1986) 1115-1117.

87Gru Göller, J.R., Grün, E., Maas, D.: Calibration of the DIDSY-IPM dust detector and application to the impact ionization detectors on board the P/Halley probes. Astronomy and Astrophys. **187** (1987) 693-698.

87Kis Kissel, J., Krueger, F.R.: The organic component in dust from comet Halley as measured by the PUMA mass spectrometer on board Vega 1. Nature **326** (1987) 755-760.

87Lan Langevin, Y., Kissel, J., Bertaux, J.-L., Chassefière, E.: First statistical analysis of 5000 mass spectra of cometary grains obtained by PUMA 1 (Vega 1) and PIA (Giotto) impact ionization mass spectrometers in the compressed modes. Astron. Astrophys. **187** (1987) 779-784.

87Sol Solc, M., Kissel, J., Vanysek, V.: Carbon-isotope ratio in PUMA 1 spectra of P/Halley dust. Astronomy and Astrophysics 187 (1987) 385-387.

88Jes Jessberger, E.K., Christoforidis, A., Kissel, J.: Aspects of the major element composition of Halley's dust. Nature **332** (1988) 691-695.

89Gru Göller, J.R., Grün, E.: Calibration of the Galileo/Ulysses dust detectors with different projectile materials and at varying impact angles. Planetary and Space Science **37** (1989) 1197-1206.

89Law Lawler, M.E., Brownlee, D.E., Temple, S., Wheelock, M.M.: Iron, magnesium, and silicon in dust from Comet Halley. Icarus **80** (1989) 225-242.

89Sag Sagdeev, R.Z., Evlanov, E.N., Fomenkova, M.N., Prilutskii, O. F., Zubkov, B.V.: Small-size dust particles near Halley's Comet. Advances in Space Research 9(3) (1989) 263-267.

90Lei Leinert, Ch., Grün, E.: Interplanetary Dust. In: Physics of the Inner Heliosphere I. eds. R. Schwenn, and E. Marsch, Springer Verlag, Berlin, S. 207-275, 1990.

90Syk Sykes, M.V.: Zodiacal dust bands – Their relation to asteroid families. Icarus **85** (1990) 267-289.

90Utt Utterback, N.G., Kissel, J.: Attogram dust cloud a million kilometers from Comet Halley: Astronomical Journal **100** (1990) 1315-1322.

91Hum Humes, D.H.: Large Craters on the Meteoroid and Space Debris Impact Experiment, in LDEF, 69 months in space: first post-retrieval symposium. Edited by Arlene S. Levine. Washington, D.C.: National Aeronautics and Space Administration, 1991, Office of Management, Scientific and Technical Information Program., p.399, 1991.

91Ige Igenbergs, E., Huedepohl, A., Uesugi, K.T., Hayashi, T., Svedhem, H., Iglseder, H., Koller, G., Glasmachers, A., Grün, E., Schwehm, G., Mizutani, H., Fujimura, A., Yamamoto, T., Araki, H., Ishii, N., Yamakoshi, K., Nogami, K.: The Munich Dust Counter - A cosmic dust experiment on board of the MUSES-A mission of Japan, in: Origin and Evolution of Interplanetary Dust, eds. Levasseur-Regourd, A.C., and Hasegawa, H., Kluwer, Dordrecht, p 45-48, 1991.

91Jes Jessberger, E.K., Kissel, J.: Chemical properties of cometary dust and a note on carbon isotopes. In: Comets in the Post-Halley Era, eds. R.L. Newburn, Jr., M. Neugebauer, and J. Rahe (Dordrecht: Kluwer Acad. Publ.), pp. 1075-1092, 1991.

91Lev Levasseur-Regourd, A.C., Hasegawa, H. (eds.): Origin and Evolution of Interplanetary Dust, Kluwer, Dordrecht, 1991.

92Gru1 Grün, E., Fechtig, H., Hanner, M.S., Kissel, J., Lindblad, B.A., Linkert, D., Morfill, G.E., Zook, H.A.: The Galileo dust detector. Space Sci. Rev. **60** (1992) 317-340.

92Gru2 Grün, E., Fechtig, H., Giese, R.H., Kissel, J., Linkert, D., Maas, D., McDonnell, J.A.M., Morfill, G.E., Schwehm, G., Zook, H.A.: The Ulysses Dust Experiment. Astron. Astrophys. Suppl. **92** (1992) 411-423.

92Law Lawler, M., Brownlee, D.: CHON as a component of dust from comet Halley. Nature **359** (1992) 810-812.

92Syk Sykes, M.V., Walker, R.G.: Cometary dust trails. I - Survey. Icarus **95** (1992) 180-210.

93Bag Baguhl, M., Grün, E., Linkert, G., Linkert, D., Siddique, N.: Identification of "small" dust impacts in the Ulysses dust detector data. Planet. Space Sci. **41** (1993) 1085-1098.

93Gru Grün, E., Zook, H.A., Baguhl, M., Balogh, A., Bame, S.J., Fechtig, H., Forsyth, R., Hanner, M.S., Horányi, M., Kissel, J., Lindblad, B.-A., Linkert, D., Linkert, G., Mann, I., McDonnell, J.A.M., Morfill, G.E., Phillips, J.L., Polanskey, C., Schwehm, G., Siddique, N., Staubach, P., Svestka, J., Taylor, A.: Discovery of jovian dust streams and interstellar grains by the Ulysses spacecraft. Nature **362** (1993) 428-430.

93Ham Hamilton, D.P.; Burns, J.A.: Ejection of dust from Jupiter's gossamer ring. Nature **364** (1993) 695-699.

93Hor1 Horányi, M., Morfill, G.E., Grün, E.: Mechanism for the acceleration and ejection of dust grains from Jupiter's magnetosphere. Nature **363** (1993) 144-146.

93Hor2 Horányi, M., Morfill, G., Grün, E.: The dusty ballerina skirt of Jupiter. J. Geophys. Res. **98(A12)** (1993) 21,245-21,251,

94Fom Fomenkova, M.N., Chang, S., Mukhin, L.M.: Carbonaceous components in the comet Halley dust. Geochim. Cosmochim. Acta **58** (1994) 4503-4512.

94Gru Grün, E., Gustafson, B., Mann, I., Baguhl, M., Morfill, G. E., Staubach, P., Taylor, A., Zook, H.A.: Interstellar dust in the heliosphere. Astronomy and Astrophysics 286 (1994) 915-924.

94Kin Kinard, W., O'Neal, R., Wilson, B., Jones, J., Levine, A., Calloway, R.: Overview of the space environmental effects observed on the retrieved Long Duration Exposure Facility (LDEF). Advances in Space Research **14(10)** (1994) 7-16.

95Bag1 Baguhl, M. Grün, E., Hamilton, D.P., Linkert, G., Riemann, R., Staubach, P.: The flux of interstellar dust observed by ULYSSES and Galileo. Space Science Reviews **72** (1995) 471-476.

95Bag2 Baguhl, M., Hamilton, D.P., Grün, E., Dermott, S.F., Fechtig, H., Hanner, M.S., Kissel, J., Lindblad, B.A., Linkert, D., Linkert, G., Mann, I., McDonnell, J.A.M., Morfill, G.E., Polanskey, C., Riemann, R., Schwehm, G., Staubach, P., Zook, H.A.: Dust measurements at high ecliptic latitudes. Science **268** (1995) 1016-1019.

95Bra Bradley J.P.: GEMS and new pre-accretionally irradiated relict grains in interplanetary dust – the plot thickens. Meteoritics **30** (1995) 491.

95Gru1 Grün, E., Baguhl, M., Hamilton, D.P., Kissel, J., Linkert, D., Linkert, G., Riemann, R.: Reduction of Galileo and Ulysses dust data. Planetary and Space Science **43** (1995) 941-951.

95Gru2 Grün, E., Baguhl, M., Kissel, J., Linkert, D., Linkert, G., Riemann, R.: Reduction of Galileo and Ulysses dust data. Planet. Space Sci **43** (1995) 941-951.

95Lov1 Love, S.G., Brownlee, D.E., King, N.L., Horz, F.: Morphology of meteoroid and debris impact craters formed in soft metal targets on the LDEF satellite. Int. J. Impact Engng., 405-405, 1995.

95Lov2 Love, S.G., Brownlee, D.E.: A direct measurement of the terrestrial mass accretion rate of cosmic dust. Science **262** (1995) 550-553.

95Tay Taylor, A.D.: The Harvard Radio Meteor Project velocity distribution reappraised. Icarus **116** (1995) 154-158.

96Cla Clarke, D., Matthews, S.A., Mundell, C.G, Weir, A.S.: On the line profiles in the spectra of the zodiacal light. Astron. Astrophys. **308** (1996) 273-278.

96Gru1 Grün, E., Baguhl, M., Riemann, R., Zook, H.A., Dermott, S., Fechtig, H., Gustafson, B.A., Hamilton, D., Hanner, M.S., Horányi, M., Khurana, K.K., Kissel, J., Kivelson, M., Lindblad, B.A., Linkert, D., Linkert, G., Mann, I., McDonnell, J.A.M., Morfill, G.E., Polanskey, C., Schwehm, G., Srama, R.: Constraints from Galileo Observations on the Origin of Jovian Dust Streams. Nature **381** (1996) 395-398.

96Gru2 Grün, E., Hamilton, D.P., Riemann, R., Dermott, S., Fechtig, H., Gustafson, B.A., Hanner, M.S., Heck, A., Horányi, M., Kissel, J., Krüger, H., Lindblad, B.A., Linkert, D., Linkert, G., Mann, I., McDonnell, J.A.M., Morfill, G.E., Polanskey, C., Schwehm, G., Srama, R., Zook, H.A.: Dust Measurements During Galileo's Approach to Jupiter and Io Encounter. Science **274** (1996) 399-401.

96Gus Gustafson, B.A.S., Hanner, M.S. (eds.): Physics, Chemistry, and Dynamics of Interplanetary Dust, Conference Series Vol. 104. Astronomical Society of the Pacific, San Francisco, 1996.

96Ham Hamilton, D.P., Grü E., Baguhl M.: Electromagnetic escape of dust from the Solar System, In: Physics, Chemistry, and Dynamics of Interplanetary Dust, ASP Conference Series, Vol. 104, Eds. B.A.S. Gustafson and Martha S. Hanner, 31-34 (1996)

96Lev Levasseur-Regourd, A.C.: Optical and Thermal Properties of Zodiacal Dust. In: B.A.S. Gustafson and M.S. Hanner (Eds.), IAU Colloq. 150: Physics, Chemistry, and Dynamics of Interplanetary Dust, Volume 104 of Astronomical Society of the Pacific Conference Series, pp. 301-308, 1996.

96Sve Svedhem, H., Münzenmayer, R., Iglseder, H.: Detection of Possible Interstellar Particles by the HITEN Spacecraft, in: Physics, chemistry, and dynamics of interplanetary dust. Astronomical Society of the Pacific Conference Series, (ASP 104), — eds. Bo A. S. Gustafson and Martha S. Hanner, p.27, 1996.

96Zoo Zook, H.A., Grün, E., Baguhl, M., Hamilton, D., Linkert, G., Liou, J.C., Forsyth, R., Phillips, J.L.: Solar wind magnetic field bending of jovian dust trajectories. Science **274** (1996) 1501-1503.

97Gru Grün, E., Staubach, P., Baguhl, M., Hamilton, D.P., Zook, H.A., Dermott S.F., Gustafson B.A., Fechtig H., Kissel J., Linkert D., Linkert G., Srama R., Hanner M.S., Polanskey C., Horanyi M., Lindblad B.A., Mann I., McDonnell J.A.M., Morfill G.E., Schwehm G.H.: South-North and Radial Traverses through the Interplanetary Dust Cloud. Icarus **129** (1997) 270-288.

97Sch Schulze, H., Kissel, J., Jessberger, E.K.: Chemistry and Mineralogy of Comet Halley's Dust, in: From Stardust to Planetesimals, Y.J. Pendleton, A.G.G.M. Tielens, ed., 397, 1997.

98Kor Kortenkamp, S.J., Dermott, S.F.: Accretion of Interplanetary Dust Particles by the Earth. Icarus **135** (1998) 469-495.

98Lei Leinert, C., Bowyer, S., Haikala, L.K., Hanner, M.S., Hauser, M.G., Levasseur-Regourd, A.-C., Mann, I., Mattila, K., Reach, W.T., Schlosser, W., Staude, H.J., Toller, G.N., Weiland, J.L., Weinberg, J.L., Witt, A.N.: The 1997 reference of diffuse night sky brightness. Astron. Astrophys. Suppl. Series **127** (1998) 1-99.

98Gru Grün, E., Krüger, H., Graps, A.L., Hamilton, D.P., Heck, A., Linkert, G., Zook, H.A., Dermott, S., Fechtig, H., Gustafson, B.A., Hanner, M.S., Horányi, M., Kissel, J., Lindblad, B.A., Linkert, D., Mann, I., McDonnell, J.A.M., Morfill, G.E., Polanskey, C., Schwehm, G., Srama, R.: Galileo observes electromagnetically coupled dust in the Jovian magnetosphere. J. Geophys. Res. **103** (1998) 20,011-20,022.

98Ige Igenbergs, E., Sasaki, S., Münzenmayer, R., Ohashi, H., Färber, G., Fischer, F., Fujiwara, A., Glasmachers, A., Grün, E., Hamabe, Y., Iglseder, H., Klinge, D., Miyamoto, H., Mukai, T., Naumann, W., Nogami, K., Schwehm, G., Svedhem, H., Yamakoshi, K.: Mars Dust Counter. Earth Planets Space **50** (1998) 241-245.

98Kel1 Kelsall, T., Weiland, J.L., Franz, B.A., Reach, W.T., Arendt, R.G., Dwek, E., Freudenreich, H.T., Hauser, M.G., Moseley, S.H., Odegard, N.P., Silverberg, R.F., Wright, E.L.: The COBE Diffuse Infrared Background Experiment Search for the Cosmic Infrared Background. II. Model of the Interplanetary Dust Cloud. Astrophys. J. **508** (1998) 44-73.

98Kel2 Kelsall, T., Weiland, J.L., Franz, B.A., Reach, W.T., Arendt, R.G., Dwek, E., Freudenreich, H.T., Hauser, M.G., Moseley, S.H., Odegard, N. P., Silverberg, R.F., Wright, E.L.: The COBE Diffuse Infrared Background Experiment Search for the Cosmic Infrared Background. II. Model of the Interplanetary Dust Cloud. The Astrophysical Journal **508** (1998) 44-73.

98Kor Kortenkamp, S.J., Dermott, S.F.: Accretion of Interplanetary Dust Particles by the Earth. Icarus **135** (1998) 469-495.

98Lan Landgraf, M., Grün, E.: In: The Local Bubble and Beyond, D. Breitschwerdt, M.J. Freyberg, and J. Trümper, eds, Lecture Notes in Physics, Vol. 506, Springer Heidelberg, 381-384, 1998.

98McD McDonnell, J.A.M., Gardner, D.J.: Meteoroid Morphology and Densities: Decoding Satellite Impact Data. Icarus **133** (1998) 25-35.

98Rie Rietmeijer, F.J.M.: Interplanetary dust particles, in: Planetary Materials, J.J. Papike ed., Review in Mineralogy Vol. 36, Mineralogical Soc. of America, Washington, p. 2-01 - 2-95, 1998.

98Tay Taylor, A.D., Elford, W.G.: Meteoroid orbital element distributions at 1 AU deduced from the Harvard Radio Meteor Project observations. Earth, Planets and Space **50** (1998) 569-575.

99Bra Bradley, J.P., Keller, L.P., Snow, T.P., Hanner, M.S., Flynn, G.J., Gezo, J.C., Clemett, S.J., Brownlee, D.E., Bowey, J.E.: An infrared spectral match between GEMS and interstellar grains. Science **285** (1999) 1716-1718.

99Fri Frisch, P.C., Dorschner, J.M., Geiss, J., Greenberg, J.M., Grün, E., Landgraf, M., Hoppe, P., Jones, A.P., Krätschmer, W., Linde, T.J., Morfill, G.E., Reach, W., Slavin, J.D., Svestka, J., Witt, A.N., Zank, G.P.: Dust in the Local Interstellar Wind, Astrophysical Journal **525** (1999) 492-516.

99Lan Landgraf, M., Augustsson, K., Grün, E., Gustafson, B.Å.S.: Deflection of the local interstellar dust flow by solar radiation pressure. Science **286** (1999) 2319-2322.

99Tay Taylor, E.A., Shrine, N.R.G., McBride, N., Green, S.F., McDonnell, J.A.M., Drolshagen, G.: Impacts on HST and Eureca solar arrays compared with LDEF using a new glass-to-aluminium conversion. Advances in Space Research **23(1)** (1999) 83-87.

99Weh Wehry, A., Mann, I.: Identification of beta-meteoroids from measurements of the dust detector onboard the ULYSSES spacecraft. Astronomy and Astrophysics **341** (1999) 296-303.

00Gra Graps, A.L., Grün, E., Svedhem, H., Krüger, H., Horányi, M., Heck, A., Lammers, S.: Io as a Source of the Jovian Dust Streams Nature **405** (2000) 48-50.

00Lan Landgraf, M.: Modeling the motion and distribution of interstellar dust inside the heliosphere. Journal of Geophysical Research **105** (2000) 10303-10316.

00Lan Landgraf, M., Baggaley, W.J., Grün, E., Krüger, H., Linkert, G.: Aspects of the mass distribution of interstellar dust grains in the Solar System from in situ measurements. J. Geophys. Res. 105 (2000) 10343-10352.

00Man Mann, I., Kimura, H.: Interstellar dust properties derived from mass density, mass distribution, and flux rates in the heliosphere. Journal of Geophysical Research **105(A5)** (2000) 10,317-10,328.

01Aue Auer, S.: Instrumentation, in "Interplanetary Dust", eds. Grün, E., Gustafson, B.A.S., Dermott, S., and Fechtig, H., Springer, Heidelberg, p 385-444, 2001.

01Bag Baggaley, W. J.: The AMOR radar: an efficient tool for meteoroid research. Advances in Space Research **28(9)** (2001) 1277-1282.

01Gru1 Grün E., Gustafson, B.A.S., Dermott, S., Fechtig, H. (eds.): Interplanetary Dust, Springer, Heidelberg, 2001.

01Gru2 Grün, E., Baguhl, M., Svedhem, H., Zook, H.A.: In-Situ Measurements of Cosmic Dust, In: Interplanetary Dust. (Eds.) E. Grün, B.A.S. Gustafson, S. Dermott, H. Fechtig, Springer, Berlin, Heidelberg, New York, 295-346 (2001).

01Jes Jessberger, E.K., Stephan, T., Rost, D., Arndt, P., Maetz, M., Stadermann, F.J., Brownlee, D.E., Bradley, J.P., Kurat G.: Properties of Interplanetary Dust: Information from Collected Samples, in: Interplanetary Dust, eds. Grün, E., Gustafson, B.A.S., Dermott, S., Fechtig, H., Springer, Heidelberg, p 253-293, 2001.

01Lev Levasseur-Regourd, A.C., Mann, I., Dumont, R., Hanner, M.S., Optical and thermal properties of interplanetary dust, in: Interplanetary Dust, eds. Grün, E., Gustafson, B.A.S., Dermott, S., and Fechtig, H., Springer, Heidelberg, 57-94, 2001.

01McD McDonnel, J.A.M, McBride, N., Green, S.F., Ratcliff, P.R., Gardner, D.J., G. Andrew D.: Near Earth Environment, in: Interplanetary Dust, eds. Grün, E., Gustafson, B.A.S., Dermott, S., and Fechtig, H., Springer, Heidelberg, p. 163-232, 2001.

01Sek Sekanina, Z., Hanner, M.S., Jessberger, E.K., Fomenkova, M.N.: Cometary Dust, in: Interplanetary Dust, eds. Grün, E., Gustafson, B.A.S., Dermott, S., Fechtig, H., Springer, Heidelberg, 95-161, 2001.

02Lei Leinert, C., Ábrahám, P., Acosta-Pulido, J., Lemke, D., Siebenmorgen, R.: Mid-infrared spectrum of the zodiacal light observed with ISOPHOT. Astron. Astrophys. **393** (2002) 1073-1079.

02Dik Dikarev, V., Grün, E.: New information recovered from the Pioneer 11 meteoroid experiment data. Astron. Astrophys. **383** (2002) 302-308.

02Gre Green S.F., Williams I.P., McDonnell J.A.M., and McBride, N. (eds.): Dust in the Solar System and Other Planetary Systems, Pergamon, Amsterdam, 2002.

02Lei Leinert, Ch., Ábrahám, P., Acosta-Pulido, J., Lemke, D., Siebenmorgen, R.: Mid-infrared spectrum of the zodiacal light observed with ISOPHOT. Astronomy and Astrophysics **393** (2002) 1073-1079.

03Alt Altobelli, N., Kempf, S., Landgraf, M., Srama, R., Dikarev, V., Krüger, H., Moragas-Klostermeyer, G., Grün, E.: Cassini between Venus and Earth: Detection of interstellar dust. Journal of Geophysical Research **108** (2003) DOI 10.1029/2003JA009874.

03Bro Brownlee, D.E., Tsou, P., Anderson, J.D., Hanner, M.S., Newburn, R.L., Sekanina, Z., Clark, B.C., Hörz, F., Zolensky, M.E., Kissel, J., McDonnell, J.A.M., Sandford, S.A., Tuzzolino, A.J.: Stardust: Comet and interstellar dust sample return mission. Journal of Geophysical Research **108** (2003) DOI 10.1029/2003JE002087.

03Cze Czechowski, A., Mann, I.: Penetration of interstellar dust grains into the heliosphere. Journal of Geophysical Research **108(A10)** (2003) 8038, DOI 10.1029/2003JA009,917.

03Kis Kissel J., Glasmachers, A., Grün, E., Henkel, H., Höfner, H., Haerendel, G., von Hoerner, H., Hornung, K., Jessberger, E.K., Krueger, F.R., Möhlmann, D., Greenberg, J.M., Langevin, Y., Silen, J., Brownlee, D., Clark, B.C., Hanner, M.S., Hoerz, F., Sandford, S., Sekanina, Z., Tsou, P., Utterback, N.G., Zolensky, M.E., Heiss, C.: Cometary and Interstellar Dust Analyzer for comet Wild 2. Journal of Geophysical Research **108(E10)** (2003) 8114, doi:10.1029/2003JE002091.

03Kru1 Krüger, H., Geissler, P., Horányi, M., Graps, A.L., Kempf, S., Srama, R., Moragas-Klostermeyer, G., Moissl, R., Johnson, T.V., Grün, E.: Jovian dust streams: A monitor of Io's volcanic plume activity, Geophysical Research Letters. **30(21)** (2003) pp. SSC 3-1, CiteID 2101, DOI 10.1029/2003GL017827

03Kru2 Krüger, H., Horányi, M., Grün, E.: Jovian dust streams: Probes of the Io plasma torus, Geophysical Research Letters **30(2)** (2003) pp. 30-1, CiteID 1058, DOI 10.1029/2002GL015920.

03Lan Landgraf, M., Krüger, H., Altobelli, N., Grün, E.: Penetration of the heliosphere by the interstellar dust stream during solar maximum. Journal of Geophysical Research **108(A10)** (2003) 8030, DOI 10.1029/2003JA009872.

03Tso Tsou, P., Brownlee, D.E., Sandford, S.A., Hörz, F., Zolensky, M.E.: Wild 2 and interstellar sample collection and Earth return. Journal of Geophysical Research **108** (2003) DOI 10.1029/2003JE002109.

03Tuz Tuzzolino, A.J., Economou, T.E., McKibben, R.B., Simpson, J.A., McDonnell, J.A.M., Burchell, M.J., Vaughan, B.A.M., Tsou, P., Hanner, M.S., Clark, B.C., Brownlee, D.E.: Dust Flux Monitor Instrument for the Stardust mission to comet, Wild 2. Journal of Geophysical Research **108(E10)** (2003) 8115, doi:10.1029/2003JE002086.

04Bro Brown, P., Jones, J., Weryk, R.J., Campbell-Brown, M.D.: The Velocity Distribution of Meteoroids at the Earth as Measured by the Canadian Meteor Orbit Radar (CMOR). Earth, Moon, and Planets **95(1-4)** (2004) 617-626.

04Gal Galligan, D.P., Baggaley, W.J.: The orbital distribution of radar-detected meteoroids of the Solar system dust cloud. Monthly Notices of the Royal Astronomical Society **353(2)** (2004) 422-446.

04Kis Kissel, J., Krueger, F.R., Silen, J., Clark, B.C.: The Cometary and Interstellar Dust Analyzer at Comet 81P/Wild 2. Science **304** (2004) 1774-1776.

04Kru Krueger, F.R., Werther, W., Kissel, J., Schmid E.R.: Assignment of quinone derivatives as the main compound class composing 'interstellar' grains based on both polarity ions detected by the 'Cometary and Interstellar Dust Analyser' (CIDA) onboard the spacecraft STARDUST, Rapid Commun. Mass Spectrom. **18** (2004) 103-111.

04Man Mann, I., Kimura, H., Biesecker, D.A., Tsurutani, B.T., Grün, E., McKibben, R.B., Liou, J.-C., MacQueen, R.M., Mukai, T., Guhathakurta, M., Lamy, P.: Dust Near The Sun. Space Science Reviews **110** (2004) 269-305.

04Sra Srama, R., Bradley, J.G., Grün, E., Ahrens, T.J., Auer, S., Cruise, M., Fechtig, H., Graps, A., Havnes, O., Heck, A., Helfert, S., Igenbergs, E., Jessberger, E.K., Johnson, T.V., Kempf, S., Krüger, H., Lamy, P., Landgraf, M., Linkert, D., Lura, F., McDonnell, J.A.M., Möhlmann, D., Morfill, G.E., Schwehm, G.H., Stübig, M., Svestka, J., Tuzzolino, A.J., Wäsch, R., Zook, H.A.: The Cassini Cosmic Dust Analyzer. Space Sci. Rev., **114(1-4)** (2004) 465-518.

04Weh Wehry, A., Krüger, H., Grün, E.: Analysis of Ulysses data: Radiation pressure effects on dust particles. Astronomy and Astrophysics **419** (2004) 1169-1174.

05Alt Altobelli, N., Kempf, S., Krüger, H., Landgraf, M., Roy, M., Grün, E.: Interstellar dust flux measurements by the Galileo dust instrument between the orbits of Venus and Mars. Journal of Geophysical Research **110** (2005) DOI 10.1029/2004JA010772.

05Dik Dikarev, V., Grün, E., Baggaley, J., Galligan, D., Landgraf, M., Jehn, R.: The new ESA meteoroid model. Advances in Space Research **35** (2005) 1282-1289.

05Gru Grün, E., Srama, R., Krüger, H., Kempf, S., Dikarev, V., Helfert, S., Moragas-Klostermeyer, G.: 2002 Kuiper prize lecture: Dust Astronomy. Icarus **174** (2005) 1-14.

05Jon Jones, J., Brown, P., Ellis, K.J., Webster, A.R., Campbell-Brown, M.D., Krzemenski, Z., Weryk, R.J.: The Canadian Meteor Orbit Radar (CMOR): System Overview and Preliminary Results. Planetary and Space Science **53** (2005) 413-421.

05Kea Kearsley, A.T., Drolshagen, G., McDonnell, J.A.M., Mandeville, J.-C., Moussi, A.: Impacts on Hubble Space Telescope solar arrays: Discrimination between natural and man-made particles, Advances in Space Research **35(7)** (2005) 1254-1262.

05Kem1 Kempf, S., Srama, R., Horányi, M., Burton, M., Helfert, S., Moragas-Klostermeyer, G., Roy, M., Grün, E.: High-velocity streams of dust originating from Saturn. Nature **433** (2005) 289-291.

05Kem2 Kempf, S., Srama, R., Postberg, F., Burton, M., Green, S.F., Helfert, S., Hillier, J.K., McBride, N., McDonnell, J.A.M., Moragas-Klostermeyer, G., Roy, M., Grün, E., Composition of saturnian stream particles. Science **307** (2005) 1274-1276.

05Kru1 Krüger, H., Linkert, G., Linkert, D., Moissl, R., Grün, E.: Galileo long-term dust monitoring in the jovian magnetosphere. Planetary and Space Science 53(11) (2005) 109-1120.

05Kru2 Krüger, H., Grün, E.: Dust Measurements During Ulysses' 2nd Jupiter Encounter, Workshop on Dust in Planetary Systems (ESA SP-643). September 26-30 2005, Kauai, Hawaii. Editors: Krueger, H. and Graps, A., p.69-72, 2007.

05Sra Srama, R., Srowig, A., Rachev, M., Grün, E., Auer, S., Conlon, T., Glasmachers, A., Harris, D., Helfert, S., Kempf, S., Linnemann, H., Moragas-Klostermeyer, G., Tschernjawski, V.: Development of an Advanced Dust Telescope. Earth, Moon and Planets, DOI: 10.1007/s11038-005-9040-z (2005).

05Tri Trigo-Rodríguez, J.M., Betlem, H., Lyytinen, E.: Leonid Meteoroid Orbits Perturbed by Collisions with Interplanetary Dust. Astrophys. J. **621** (2005) 1146-1152.

06Alt Altobelli, N., Grün, E., Landgraf, M.: A new look into the Helios dust experiment data: presence of interstellar dust inside the Earth's orbit. Astronomy and Astrophysics **448(1)** (2006) 243-252.

06Bro Brownlee, D.E., Tsou, P., Aléon, J., et al.: Comet 81P/Wild 2 Under a Microscope. Science **314(5806)** (2006) 1711- 1716.

06Fly Flynn, G.J., Bleuet, P., Borg, J., Bradley, J.P., Brenker, F.E., Brennan, S., Bridges, J., Brownlee, D.E., et al.: Elemental Compositions of Comet 81P/Wild 2 Samples Collected by Stardust. Science **314(5806)** (2006) 1731-1735.

06Hor Hörz, F., Bastien, R., Borg, J., Bradley, J.P.: Impact Features on Stardust: Implications for Comet 81P/Wild 2 DustBridges. Science **314(5806)** (2006) 1716-1719.

06Kel Keller, L.P., Bajt, S., Baratta, G.A., Borg, J., Bradley, J.P., Brownlee, D.E., et al.: Infrared Spectroscopy of Comet 81P/Wild 2 Samples Returned by Stardust. Science 314(5806) (2006) 1728-1731.

06Kli Klinkrad, H.: The current space debris environment and its sources, in Space Debris Models and Risk Analysis, ed. H. Klinkrad, Springer Praxis Publ., Chichester, p. 5-58, 2006.

06Kru1 Krüger, H., Graps, A. (eds.): Dust in Planetary Systems, ESA SP-643, ESA Publications Division, Noordwijk, 2006.

06Kru2 Krüger, H., Altobelli, N., Anweiler, B., Dermott, S.F., Dikarev, V., Graps, A.L., Grün, E., Gustafson, B.A., Hamilton, D.P., Hanner, M.S., Horányi, M., Kissel, J., Landgraf, M., Lindblad, B.A., Linkert, D., Linkert, G., Mann, I., McDonnell, J.A.M., Morfill, G.E., Polanskey, C., Schwehm, G., Srama, R., Zook, H.A.: Five years of Ulysses dust data: 2000 - 2004. Planetary and Space Science **54** (2006) 932-956.

06Kru3 Krüger, H., Graps, A.L., Hamilton, D.P., Flandes, A., Forsyth, R.J., Horányi, M., Grün, E.: Ulysses jovian latitude scan of high-velocity dust streams originating from the jovian system. Planetary and Space Science **54(9-10)** (2006) 919-931.

06McK McKeegan, K.D., Aléon, J., Bradley, J., Brownlee, D., et al.: Isotopic Compositions of Cometary Matter Returned by Stardust. Science **314(5806)** (2006) 1724-1728.

06Pos Postberg, F., Kempf, S., Srama, R., Green, S.F., Hillier, J.K., McBride, N., Grün, E.: Composition of jovian dust stream particles. Icarus **183** (2006) 122-134.

06San Sandford, S.A., Aléon, J., Alexander, C.M. O.'D., Araki, T., Bajt, S., Baratta, G.A., Borg, J., Bradley, J.P., Brownlee, D.E., et al.: Organics Captured from Comet 81P/Wild 2 by the Stardust Spacecraft. Science 314(5806) (2006) 1720-1724.

06Spa Spahn, F., Schmidt, J., Albers, N., Hörning, M., Makuch, M., Seiß, M., Kempf, S., Srama, R., Dikarev, V., Helfert, S., Moragas-Klostermeyer, G., Krivov, A.V., Sremčević, M., Tuzzolino, A.J., Economou, T., Grün, E.: Cassini Dust Measurements near Enceladus and Implications for Saturn's E Ring. Science **311** (2006) 1416-1418.

06Sra1 Srama R., Kempf, S., Moragas-Klostermeyer, G. et al.: Laboratory Tests of the Large Mass Analyzer, in: Dust in Planetary Systems, eds. Krüger, H., Graps, A., ESA SP-643, ESA Publications Division, Noordwijk, p. 209-212 (2006).

06Sra2 Srama, R., Srowig, A., Auer, S. et al.: A Trajectory Sensor for Sub-Micron Sized Dust, in: Dust in Planetary Systems, eds. Krüger, H., Graps, A., ESA SP-643, ESA Publications Division, Noordwijk, 213-217 (2006).

06Zol Zolensky, M.E., Zega, T.J., Yano, H., Wirick, S., Westphal, A.J., Weisberg, M.K., et al.: Mineralogy and Petrology of Comet 81P/Wild 2 Nucleus Samples. Science 314(5806) (2006) 1735-1739. .

07Hil1 Hillier, J.K., Green, S.F., McBride, N., Altobelli, N., Postberg, F., Kempf, S., Schwanethal, J.P., Srama, R., McDonnell, J.A.M., Grün, E.: Interplanetary dust detected by the Cassini CDA Chemical Analyser. Icarus **190** (2007) 643-654.

07Hil2 Hillier, J.K., Green, S.F., McBride, N., Schwanethal, J.P., Postberg, F., Srama, R., Kempf, S., Moragas-Klostermeyer, G., McDonnell, J.A.M., Grün, E.: The composition of Saturn's E ring. Mon. Not. R. Astron. Soc. **377** (2007) 1588-1596.

07Hor Horányi, M., Hoxie, V., James, D., Poppe, A., Bryant, C., Grogan, B., Lamprecht, B., Mack, J., Bagenal, F., Batiste, S., Bunch, N., Chanthawanich, T., Christensen, F., Colgan, M., Dunn, T., Drake, G., Fernandez, A., Finley, T., Holland, G., Jenkins, A., Krauss, C., Krauss, E., Krauss, O., Lankton, M., Mitchell, C., Neeland, M., Reese, T., Rash, K., Tate, G., Vaudrin, C., Westfall, J.: The Student Dust Counter on the New Horizons Mission, Space Sci. Rev. Online First (2007) DOI 10.1007/s11214-007-9250-y.

07Kru Krüger, H., Landgraf, M., Altobelli, N., Grün, E.: Interstellar Dust in the Solar System. Space Science Reviews **130** (2007) 401-408.

07Rea Reach, W.T., Kelley, M.S., Sykes, M.V.: A survey of debris trails from short-period comets. Icarus **191** (2007) 298-322.

07Ste Sternovsky, Z., Amyx, K., Bano, G., Landgraf, M., Horanyi, M., Knappmiller, S., Robertson, S., Grün, E., Srama, R., Auer, S.: The Large Area Mass Analyzer (Lama) Instrument for the Chemical Analysis of Interstellar Dust Particles. Rev. Sci. Instrum. **78** (2007) 014501.

08Dro Drolshagen, G.: Impact effects from small size meteoroids and space debris, Advances in Space Research **41(7)** (2008) 1123-1131.

08Ipa Ipatov, S.I., Kutyrev, A.S., Madsen, G.J., Mather, J.C., Moseley, S.H., Reynolds, R.J.: Dynamical zodiacal cloud models constrained by high resolution spectroscopy of the zodiacal light. Icarus **194** (2008) 769-788.

08Pos Postberg, F., Kempf, S., Hillier, J.K., Srama R., Green S.F, McBride N., Grün, E.: The E-ring in the vicinity of Enceladus II. Probing the moon's interior—The composition of E-ring particles. Icarus **193** (2008) 438-454.